ASNC imaging guidelines/SNMMI procedure standard for positron emission tomography (PET) nuclear cardiology procedures

Vasken Dilsizian, MD,[a] Stephen L. Bacharach, PhD,[b] Rob S. Beanlands, MD,[c] Steven R. Bergmann, MD, PhD,[d] Dominique Delbeke, MD,[e] Sharmila Dorbala, MD, MPH,[f] Robert J. Gropler, MD,[g] Juhani Knuuti, MD, PhD,[h] Heinrich R. Schelbert, MD, PhD,[i] and Mark I. Travin, MD[j]

[a] Department of Diagnostic Radiology and Nuclear Medicine, University of Maryland School of Medicine, Baltimore, MD
[b] Department of Radiology, University of California-San Francisco, San Francisco, CA
[c] Division of Cardiology, University of Ottawa Heart Institute, Ottawa, Canada
[d] Pat and Jim Calhoun Cardiology Center, UConn Health, Farmington, CT
[e] Department of Radiology, Vanderbilt University Medical Center, Nashville, TN
[f] Division of Nuclear Medicine, Brigham and Women's Hospital, Boston, MA
[g] Division of Nuclear Medicine, Washington University School of Medicine, St. Louis, MO
[h] Turku PET Centre, Turku University Hospital, Turku, Finland
[i] Department of Molecular and Medical Pharmacology, David Geffen School of Medicine at UCLA, Los Angeles, CA
[j] Department of Radiology, Montefiore Medical Center, Bronx, NY

Received Mar 25, 2016; accepted Mar 25, 2016
doi:10.1007/s12350-016-0522-3

INTRODUCTION

Stress-induced myocardial perfusion defects have been firmly established as an important diagnostic and prognostic technique for identifying flow-limiting epicardial coronary artery disease (CAD). However, interpretation of such myocardial perfusion imaging (MPI) studies has been primarily qualitative or semi-quantitative in nature, assessing regional perfusion defects in relative terms. Quantitative positron emission tomography (PET) measurements of myocardial blood flow (MBF) in absolute terms (milliliters per gram per minute) offer a paradigm shift in the evaluation and management of patients with CAD. The latter is concurrent with the recent shift in the management of CAD from an anatomical gold standard (i.e., coronary angiogram) to a functional one. Moreover, non-invasive quantification of MBF extends the scope of conventional MPI from detection of end-stage, advanced, and flow-limiting epicardial CAD to early stages of atherosclerosis or microvascular dysfunction and assessment of balanced reduction of MBF in all three major coronary arteries. Quantitative approaches that measure MBF with PET identify multivessel CAD and offer the opportunity to monitor responses to lifestyle and/or risk factor modification and to therapeutic interventions.

PET utilizes radionuclide tracer techniques to produce images of in vivo radionuclide distribution using an external detector system. Similar to computed tomography (CT), the images acquired with PET represent cross-sectional slices through the heart. However, with PET, the image intensity reflects organ function and physiology as opposed to anatomy. The functional

This article is co-sponsored by the American Society of Nuclear Cardiology and the Society of Nuclear Medicine and Molecular Imaging. The full set of guidelines can be found within this article, published in the Journal of Nuclear Cardiology; a related Editorial, published in the Journal of Nuclear Medicine, can be found at: https://doi.org/10.2967/jnumed.116.176214.

Reprint requests: Vasken Dilsizian, MD, Department of Diagnostic Radiology and Nuclear Medicine, University of Maryland Medical Center, South Greene Street, Rm N2W78, Baltimore, MD 21201-1595; *vdilsizian@umm.edu*

J Nucl Cardiol 2016;23:1187–226.
1071-3581/$34.00

information that can be obtained from PET images depends upon the radiopharmaceutical employed. PET allows non-invasive evaluation of MBF, function, and metabolism using physiological substrates prepared with positron-emitting radionuclides, such as carbon, oxygen, nitrogen, and fluorine. These radionuclides have half-lives that are often considerably shorter than those used in single photon emission computed tomography (SPECT). Positron-emitting radionuclides can be produced using a cyclotron (e.g., ^{18}F-fluoro-2-deoxyglucose [^{18}F-FDG] with a 110-minute half-life) or using a generator (e.g., rubidium-82 [^{82}Rb] with a 75-second half-life from a strontium-82 [^{82}Sr] generator).

PET radionuclides reach a more stable configuration by the emission of a positron. Positrons are the antimatter of electrons. They are positively charged particles with the same rest mass as electrons. When a positron spends time near an electron, the two annihilate—they both disappear and in their place two 511-keV gamma rays are emitted. Because the gamma rays are nearly collinear (discharged at 180° to each other) and travel in opposite directions, the PET detectors can be programmed to register only events with temporal coincidence of photons that strike directly at opposing detectors.[1] The result is improved spatial (4- to 6-mm) resolution when compared with SPECT, as well as temporal resolution. The high temporal resolution of PET is also explained by the fact that the imaging device is stationary compared with the rotating imaging gantry for SPECT. Moreover, the PET system is more sensitive than a SPECT system due to the higher count rate and provides the possibility of attenuation correction. The result of these advantages with PET is the potential for quantitation of tracer concentration in absolute units. Quantification of MBF may provide diagnostic and prognostic information earlier than visual interpretation of relative radiotracer uptake, which is a fundamental disadvantage of the conventional SPECT technique.

The PET detectors are placed in a ring, surrounding the patient, and are configured to register only photon pairs that strike opposing detectors at approximately the same time, termed coincidence detection. Over the course of a typical scan, millions of coincidence events are recorded, and projections of the activity distribution are measured at all angles around the patient. These projections are subsequently used to reconstruct an image of the in vivo radionuclide distribution using the same algorithms as those used in SPECT and x-ray CT. The resulting PET images have improved spatial and temporal resolution when compared to SPECT. Hence, the imaging properties of PET meet some of the Centers for Medicare & Medicaid Services (CMS) implementation of quality initiatives to assure quality health care. PET MPI is effective (high diagnostic accuracy), safe (low radiation exposure), efficient (short image acquisition times), and patient-centered (accommodates ill or higher risk patients, as well as those with large body habitus), providing equitable and timely care.

Recent advances in hybrid PET/CT instrumentation and multichannel spiral CT allow detailed, non-invasive visualization of the coronary arteries, as an adjunct to PET imaging. Whereas multichannel CT angiography provides information on the presence and extent of anatomical luminal narrowing of epicardial coronary arteries, stress myocardial perfusion PET provides information on the downstream functional consequences of such anatomic lesions. Thus, with hybrid PET/CT systems, complementary information of anatomy and physiology can be obtained during the same imaging session. The ability to evaluate CAD, myocardial perfusion, metabolic viability, and ventricular function from a hybrid PET/CT image makes such systems an important tool in the clinical practice of cardiology.

In the last few years, not only have combined PET/CT scanners proliferated, but PET combined with magnetic resonance (MR) imaging scanners have been introduced (PET/MR). While the main use for these scanners continues to be for oncological applications, cardiac CT and MR are now well established. The melding of CT or MR to a PET camera increases the complexity of scanning protocols, quality maintenance and assurance but also expands imaging to correlate anatomy, molecular biology, and metabolism with nuclear imaging thereby providing comprehensive evaluation of the heart. For example, co-registration of ^{18}F-FDG metabolic imaging with morphological, functional, and tissue imaging attributes of MR presents new opportunities for disease characterization, such as cardiac sarcoidosis, hallmarked by inflammatory injury, non-caseating granuloma formation, and organ dysfunction which could be the first clinical application of PET/MR in cardiology.[2] ^{18}F-FDG PET in cardiac sarcoidosis produces ''hot spot'' images. MR is particularly helpful for anatomic co-localization of the ^{18}F-FDG PET signal within the heart, reflecting the inflammatory phase of cardiac sarcoidosis. MR delayed enhancement, on the other hand, provides information on areas of fibrosis and scar as a consequence of cardiac sarcoidosis. It is reasonable, therefore, to have a hybrid system in which MR can show the focus of prior injury or scar from sarcoidosis superimposed on inflammatory markers seen with ^{18}F-FDG.[3]

The current document is an update of an earlier version of PET guidelines that was developed by the American Society of Nuclear Cardiology (ASNC).[4] The publication is designed to provide imaging guidelines for physicians and technologists who are qualified to practice nuclear cardiology. While the information supplied

in this document has been carefully reviewed by experts in the field, the document should not be considered medical advice or a professional service. We are cognizant that PET, PET/CT, and PET/MR technology is evolving rapidly and that these recommendations may need further revision in the near future. Hence, the imaging guidelines described in this publication should not be used in clinical studies until they have been reviewed and approved by qualified physicians and technologists from their own particular institutions.

PET, PET/CT, AND PET/MR INSTRUMENTATION

PET Imaging Systems

The majority of dedicated PET cameras consist of rings of small detectors that are typically a few millimeters on a side, and tens of millimeters deep. Coincidences between detectors in a single ring produce one tomographic slice of data. Usually, one or more adjacent rings may also contribute to counts in that slice. In a 2-dimensional (2D) or ''septa-in'' PET scanner, there is a septum (e.g., lead or tungsten) between adjacent rings. This septum partially shields coincidences from occurring between detectors in one ring and detectors in a non-adjacent or more distant ring. By minimizing coincidences between a ring and its more distant neighboring rings, the septa greatly reduce scattered events.

A scanner with no septa in place is referred to as a 3-dimensional (3D) or ''septa-out'' scanner. This nomenclature is somewhat confusing as both septa-in and septa-out modes produce 3D images. The septa-out (3D) mode, however, permits coincidences between all possible rings, greatly increasing sensitivity but also greatly increasing scatter, as well as the count rate for each individual detector. This increase in count rate can increase dead time and random events. The increased sensitivity is the greatest for the central slice and falls rapidly and roughly linearly, for slices more distant from the central slice. The slices near the edge have a sensitivity about the same as in a 2D scanner but with greater scatter. Scatter is measured with standards provided by the National Electrical Manufacturers Association (NEMA)[5–9] and is typically in the order of 10 to 15% for 2D scanners and 30-40% or more for 3D scanners. In chest slices encompassing the heart, as opposed to the relatively small NEMA phantom, there is an even larger increase in scattered counts for 3D imaging. For cardiac applications, scatter tends to artifactually increase the counts in cold areas surrounded by higher activity regions (e.g., a defect surrounded by normal uptake, or near the liver).

Some scanners have retractable septa, permitting the user to choose between 2D and 3D operation. Many PET/CT manufacturers have opted for scanners that operate only in 3D mode, because these allow maximum patient throughput for multi-bed position oncology studies. Situations in which 3D mode may be advantageous include the following:

1. Whole-body patient throughput is important (e.g., a busy oncology practice).
2. Radiation exposure is critical, so that reductions in injected activity are desired.
3. Special (i.e., usually research) radiopharmaceuticals are being used, which can only be produced in low-radioactivity quantities.

As noted above, although 3D acquisition is in principle many times more sensitive than 2D, ''accidental,'' or random coincidences (termed randoms), dead time, and scatter can greatly reduce the effective sensitivity of images acquired in 3D, especially at high doses. Thus, in order to prevent poor-quality images, lower doses are often administered in 3D mode. Accordingly, 3D imaging can be used when the dose must be minimized (e.g., in normal volunteers, in children, or when multiple studies are planned) or when scatter is minimal (e.g., brain imaging). The advent of lutetium-based crystals, such as lutetium oxyorthosilicate (LSO) and lutetium yttrium orthosilicate (LYSO) along with gadolinium oxyorthosilicate (GSO)-based PET scanners, and even bismuth germanate (BGO) scanners with new-generation optimized photomultiplier/crystal coupling schemes and high-speed electronics, has made 3D imaging more practical. Improvements in software, coupled with improvements in electronics and crystal technology, can, in part, compensate for the increase in randoms, dead time, and scattered events associated with 3D imaging.[10] The use of 3D-cardiac imaging with new-generation machines continues to be evaluated. The degree to which any of these improvements in 3D is achieved in practice for cardiac imaging may vary between manufacturers and between applications (high-count rate versus normal count rate studies).

PET Imaging: Crystal Types

Three different crystal types are commonly employed in PET, including BGO, GSO, and lutetium-based crystals, such as LSO and LYSO, although other crystal types have also been used. The technical specifications of each crystal type have been well documented.[11] Each type of crystal has been used successfully for cardiac imaging. BGO has the highest stopping power, but relatively poor energy resolution (which limits energy-based scatter reduction) and poor

timing resolution (limiting its ability to reduce randoms at high count rates). GSO, LSO, and LYSO have better timing resolution and, in theory, better energy resolution. For 2D imaging, GSO, LSO, and LYSO may not offer significant advantages over BGO, given the inherently high sensitivity of BGO and the lower count rates encountered in 2D versus 3D studies. The main advantage of the GSO and lutetium-based crystals is reduced dead time, which enables them to acquire data at higher count rates associated with operating in 3D mode, and to better minimize the effects of randoms. One minor disadvantage of LSO and LYSO is their intrinsic radioactivity, which contributes to a small increase in the random event rate.

The better energy resolution of GSO, LSO, or LYSO compared to BGO, and consequent reduction of scatter, would in principal make these detector types advantageous in 3D mode. At present, the theoretical energy resolution for these detectors does not seem to have been fully realized in practice, leaving all four crystal types with similar energy-based scatter rejection (i.e., GSO and lutetium-based crystals giving an improvement, but not a great one, over BGO) and making 2D imaging still the method of choice if scatter rejection is critical.

Modern image reconstruction algorithms incorporate improved models for scatter correction, and as a result, the impact of scatter for state-of-the-art scanners operating in 3D mode is usually acceptable for clinical imaging. In cardiac imaging, areas of low uptake (e.g., perfusion defects) may still be slightly overestimated with 3D compared to 2D when these defects are near regions of high tracer uptake. The suitability of 3D mode for cardiac PET imaging should be evaluated by the user. For studies with a wide range of count rates, such as quantitative ^{82}Rb scans, 3D acquisitions can be problematic unless great care is taken to address the high count rates achieved during and immediately after infusion. Therefore, for 3D ^{82}Rb acquisitions, GSO and lutetium-based crystals are thought to have an advantage over BGO. Improvements in crystal manufacture and design, as well as the development of scanners with new crystal types, may further improve 3D scatter rejection and 3D imaging during bolus injections (e.g., quantitative ^{82}Rb studies).

PET Time-of-Flight (TOF) Imaging

Machines that incorporate time-of-flight (TOF) information in the acquisition process have been developed and are available. TOF refers to the time difference between when the two 511-keV annihilation photons reach their respective detectors, 180° apart. For example, if the positron annihilation occurred at the center of the machine, the two photons would reach their respective detectors at exactly the same time, while if the annihilation occurred closer to one detector than the other, the photon would reach the closer detector first. If the time difference could be measured accurately enough, it would be possible to determine exactly where the annihilation event is originated.

Unfortunately, current detector and instrumentation technology is not nearly good enough to achieve this level of accuracy. However, it has been shown that adding TOF capability can improve the statistical quality of the data (i.e., the noise).[12–14] For example, recent reports indicate that TOF imaging can improve noise and image quality in ^{13}N-ammonia perfusion imaging,[15] and therefore potentially improve image quality or even perhaps, in the future, reduce the dose needed to achieve a given image quality. In addition, as mentioned above, performing high-count rate cardiac studies with 3D scanners presents difficulties. Preliminary studies indicate that some of these difficulties may be reduced with TOF imaging; however, much work remains to be done. As most users do not use machines in the TOF mode, quality control (QC) of this feature should follow recommendations of the manufacturer and NEMA NU 2-2012 testing procedures.[5]

Hybrid PET/CT and PET/MR Cameras

For many years, most PET scanners have been sold combined with a CT scanner. In all cases, the manufacturer starts with a state-of-the-art PET scanner, whose characteristics have been described in the section above. The manufacturer then adds a CT system, with 64 or more slices. These combined systems, in practice, demonstrate a range of integration. At one end of the spectrum, the hardware and software of the CT systems are completely integrated within the PET scanner. A common, unified gantry is used and a single, unified software system with an integrated PET/CT interface is provided. At the other end of the spectrum, the hardware and software of the CT system are less integrated. In some machines, a separate CT gantry is carefully placed in front of or behind the PET gantry, and a separate workstation is used to control the CT system. Although originally the CT component of the hybrid PET/CT camera was developed for attenuation correction and anatomical co-localization purposes, more modern machines have CT scanners that are of diagnostic quality, which allows the assessment of both coronary artery calcium scoring and CT angiography. The scope of these CT procedures is beyond the purview of these PET guidelines, and has been covered in a recent SNMMI/ASNC/SCCT guideline.[16] More recently, PET scanners have also been introduced combined with MR.

Two different types of systems are available—in-line systems and simultaneous systems. The first uses a common gantry for both imaging modalities, and is very similar to PET/CT devices with the CT replaced by MR. In-line systems allow existing state-of-the-art PET and MR scanners to be combined adjacently, although alterations may be necessary to accommodate the nearby high magnetic fields. The so-called ''simultaneous'' systems allow both image sets to be acquired at the same time—although depending on their design there may be some performance limitations. Attenuation correction with either type of system can be problematic. Unlike CT images, MR images do not necessarily produce images from which PET attenuation correction factors can be derived. MR imaging is, of course, quite valuable in cardiology, so it is possible that the combination of MR with PET will result in interesting new clinical applications. PET/MR is still in its early stages and much work remains before its full clinical potential in cardiology is recognized.

PET Imaging: Attenuation Correction

For dedicated PET scanners (without CT or MR), rotating rod sources or rings of germanium-68 (^{68}Ge)/gallium-68 (^{68}Ga) or cesium-137 (^{137}Cs) are used to acquire a transmission scan for attenuation correction. A typical transmission scan with rotating rods adds about 60 to 600 seconds to the overall imaging time. This is acceptable for cardiac imaging, but is a significant drawback for multi-bed position oncology scans. Because oncology applications continue to drive sales of PET scanners, manufacturers looked for a way to reduce this transmission scan time. For this reason, and because of other advantages of CT, nearly all current commercially available PET scanners are hybrid PET/CT systems. These scanners, in general, have eliminated the rotating rod source and instead rely on CT scans for attenuation correction. The Hounsfield units (HU) generated by the CT scanner can usually be accurately converted into PET attenuation values.

CT-based attenuation correction typically adds less than 10 seconds to the cardiac scan time. The use of either CT or the rotating rod for attenuation correction requires precise alignment between the transmission image and the emission image. An advantage of CT over transmission sources is a much reduced scan time, which helps reduce overall patient motion. The high speed of CT scans, however, freezes the heart and lungs at one phase of the respiratory cycle, causing potential misalignment between the CT-based transmission and emission scans. The latter, of course, are averaged over many respiratory cycles. The respiratory misalignment between the CT image and emission data can produce significant artifacts and errors in apparent uptake in the myocardial segments adjacent to lung tissue.[17] Errors in attenuation correction from misregistration are typically much worse if the CT is acquired at full inspiration, and so the CT is often acquired at either end-expiration or during shallow breathing. Software realignment must be performed to minimize any remaining misalignment. Other techniques (e.g., slow CT, respiratory gating, and 4D-CT) are under development for compensating for respiratory motion, but are still in the research phase and are not further described here.

MR images, unlike CT or rotating rod images, do not directly measure attenuation values. Instead, MR-based attenuation correction usually must rely on indirect methods, for example using the MR image to separate tissue types (e.g., lung, soft tissue, and bone). The segmented images are then used to assign each tissue type a pre-determined attenuation value. Use of this method for organs, such as the heart, with a tissue/lung interface, still requires further study.

PET AND PET/CT OR PET/MR IMAGING QC

PET QC Procedures

The procedures below should be suitable for ensuring overall proper basic operation of a PET scanner. Table 1 lists the recommended PET imaging QC schedules.[4] Note that, unlike planar and SPECT imaging, there are no widely accepted, published QC procedures for PET. Some additional procedures may be required by particular manufacturers.

Acceptance testing. It is recommended that the NEMA performance measurements, as defined by NU 2-2012,[5] be made before accepting the PET scanner. Many of these tests can be performed by the company supplying the PET scanner. If so, it is recommended that the purchaser's representatives work with the manufacturer's representatives during these tests. The NU 2-2012 recommendations have superseded the NU 2-2007 recommendations.[8] In scope, the tests are nearly equivalent between NU 2-2012 and NU 2-2007.[5,8] For cardiac imaging, these QC performance standards should be performed.

There are two reasons for making these performance measurements:

1. To ensure the new PET scanner meets specifications published by the manufacturer and
2. To provide a standard set of measurements that allows the user to document the limitations of the scanner and to provide a standard against which to track changes that may occur over time.

Table 1. Suggested QC procedures: dedicated PET imaging devices

Procedure	Frequency
Acceptance testing (NU 2-2012)[5]	Once upon delivery and upon major hardware upgrades
Daily QC, as recommended by vendor (attenuation blank scan, phantom scan, etc.)	Daily
Sensitivity and overall system performance	Weekly preferred (or at least monthly)
Accuracy (corrections for count losses and randoms)	At least annually
Scatter fraction	At least annually
Accuracy of attenuation correction	At least annually
Image quality	At least annually
Measurements specified by the manufacturer	As per the manufacturer

Daily QC scan. Each day the PET detectors should be evaluated to ensure proper operation before commencing with patient injections or scans. The daily quality procedure varies according to the design of the scanner and recommendations of the vendor. For example, some scanners use an attenuation blank scan to evaluate detector constancy, and others may use a scan of a standard phantom. In addition to numerical output of the scanners (chi-square, uniformity, etc.), the raw sinogram data also should be inspected to evaluate detector constancy.

Sensitivity. NEMA NU 2-2012 provides recommended procedures for measuring system sensitivity.[5] Subtle changes in PET system sensitivity may occur slowly over time. More dramatic changes in sensitivity may reflect hardware or software malfunction. There are simple tests designed to monitor such changes in sensitivity. Ideally, these tests should be performed weekly, but no less than monthly. For many systems, the daily QC scan also provides a measure useful for tracking changes in sensitivity.

Spatial resolution. Spatial resolution is measured using a point source as specified in the NEMA NU 2-2012.[5]

Scatter fraction. Intrinsic scatter fraction is measured according to NEMA NU 2-2012 specifications.[5]

Accuracy of attenuation correction and overall clinical image quality. Attenuation correction should be assessed using the IEC phantom, as specified in the NU 2012 recommendations.[5] If this phantom is not readily available, it is suggested that similar measurements be performed with a phantom approximating a typical human body shape and size (e.g., a 20- by 30-cm elliptical phantom or anthropomorphic phantom). It should have at least one cold sphere or cylinder and one hot sphere or cylinder, as well as some material simulating lung tissue to ensure proper performance in the presence of non-uniform attenuating substances.

Variations among manufacturers. The above recommendations regarding PET scanner quality assurance are general guidelines. In addition, each manufacturer has its own periodic QC recommendations for parameters such as ''singles'' sensitivity, coincidence timing, energy calibration, and overall system performance. These, by necessity, require different measurement protocols that may vary even between models for the same manufacturer. These measurements must be performed as detailed by the manufacturer. However, the measurements specified above are not intended to replace these basic system-specific QC measurements.

CT QC Procedures

The procedures below should be suitable for ensuring overall proper basic operation of a CT scanner. Table 2 lists recommended CT imaging QC schedules. Some additional procedures may be required by particular manufacturers.

Calibration. The reconstructed CT image must exhibit accurate, absolute CT numbers in HU. This is critical for the use of CT images for PET attenuation correction, because the quantitative CT values are transformed, usually via a bilinear or trilinear function with one hinge at or near the CT value for water, to attenuation coefficients at 511 keV. Any errors in CT numbers will be propagated as errors in estimated 511-keV attenuation coefficients, which in turn will adversely affect the attenuation-corrected PET values. CT system calibration is performed with a special calibration phantom that includes inserts of known CT numbers. This calibration is done by the manufacturer's

Table 2. CT QC procedures

Test	Requirement	Frequency
Calibration	Mandatory	Monthly*
Field uniformity	Mandatory	Monthly*
*or as recommended by the manufacturer		

field-service engineers. The CT calibration is then checked daily with a water-filled cylinder, usually 24 cm in diameter provided by the manufacturer. In practice, if the error is greater than 5 HU (i.e., different than the anticipated value of 0 HU), the CT system is considered to be out of calibration. The technologist will then usually perform an air calibration, to determine if this corrects the overall calibration (i.e., brings the CT number for water back to within 5 HU of 0). If it does not, the manufacturer's field-service engineer must be called. On an annual basis, or after any major repair or calibration, calibration is checked by the manufacturer's service engineer.

Field uniformity. The reconstructed CT image must exhibit uniform response throughout the field of view (FOV). In practice, this means a reconstructed image or a uniform water-filled cylinder must demonstrate low variation in CT number throughout this image. In practice, small circular regions of interest (ROIs) are placed at the four corners of the cylinder image, and the mean CT number is compared to that from a region in the center of the phantom; the difference in mean region CT number should not exceed 5 HU. Non-uniformities greater than this may produce sufficient quantitative inaccuracies so as to affect PET attenuation correction based on the CT image.

Table 3 lists recommended CT QC schedules for combined PET/CT units. Users should consult the manufacturer regarding the specific manner and frequency with which tests should be performed for the CT component of their PET/CT device. Both the American College of Radiology (ACR) and American Association of Physicists in Medicine (AAPM) have published CT testing procedural guidelines.[18]

Combined PET/CT QC Procedures

The PET and CT portions of the combined system should be assessed as described for the dedicated PET and CT imaging devices. In addition to the independent QC tests for the PET and CT portions of the combined system, it is necessary to perform additional tests that assess the combined use of PET and CT. Table 4 lists recommended QC procedures for combined PET/CT units.

Registration. The reconstructed PET and CT images must accurately reflect the same 3D locations (i.e., the two images must be in registration). Such registration is often difficult because the PET and CT portions of all commercial combined PET/CT systems are not coincident (i.e., the PET and CT ''slices'' are not in the same plane) and the PET and CT gantries are contiguous. In practice, this means that the PET and CT acquisitions do not simultaneously image the same slice. In fact, because the bed must travel different distances into the gantry to image the same slice in the patient for PET versus CT, there is ample opportunity for misregistration via x, y, z misalignment of bed motion—or, of perhaps even greater concern, because of differential ''bed sag'' for the PET and CT portions, depending on the table design.

In addition, electronic drift can influence the ''position'' of each image, so that calibrations for mechanical registration can become inaccurate over time. Thus, it is imperative to check PET-to-CT registration on an ongoing basis. This is usually performed with a specific phantom or jig containing an array of point sources visible in both PET and CT. Errors in co-location in the fused PET/CT images are assessed, such as by means of count profiles generated across transaxial

Table 3. Schedule of CT QC for PET/CT units

Test	Frequency
Water phantom QA	Daily
Tube warm-up	Daily
Air calibration (“fast QA)	Daily
Water phantom checks: slice thickness, accuracy, positioning	Monthly

Table 4. Combined PET/CT QC procedures

Test	Requirement
Registration	Mandatory
Attenuation correction accuracy	Mandatory

slices. Such errors, after software registration corrections, should be less than 1 mm. It is important to image this registration jig in a number of positions along the bed. It may also be helpful to place a weight on the end of the bed to produce some bed sag and repeat the assessment. The above considerations are in addition to the patient-specific alignment QC clinically necessary to assess possible patient or respiratory motion.

Attenuation correction accuracy. The use of the CT image for PET attenuation correction requires a transformation of the observed CT numbers in HU to attenuation coefficients at 511 keV. This transformation is usually accomplished with a bilinear or trilinear calibration curve, with one ''hinge'' at a CT value of 0 (i.e., hinged at the CT value for water).

At a minimum, it is important to image a water-filled cylinder to assess PET field uniformity and PET activity concentrations after CT-based PET attenuation correction. Errors in CT-to-PET attenuation transformations are usually manifest as a corrected PET image without a ''flat'' profile from edge to center (i.e., the activity at the edge is either too high or too low relative to that at the center of the phantom) and with resulting attenuation-corrected absolute PET values that are incorrect (although these values depend on absolute PET scanner calibration as well as accurate CT-based PET attenuation correction).

If possible, the CT-based attenuation-corrected PET values should be compared with those from the rotating rod source-based attenuation-corrected PET values in the same phantom. Moreover, if available, more sophisticated phantoms with variable attenuation and variable activity distributions can be used to more comprehensively assess any errors in CT-based PET attenuation correction.

The accuracy of CT attenuation-corrected PET images is still under investigation. Recent work has reported that even after correcting for potential PET/CT misalignment, tracer uptake maps derived from CT-based attenuation correction differ from those derived using transmission source correction.[17,19,20]

PET-MR QC Procedure

Many of the principles outlined above for PET/CT apply to hybrid PET/MR systems. Co-localization is especially important. Errors in misregistration of CT or MR and PET emission images can result in significant reconstruction errors. Because these scanners are still in evolution, QC from the manufacturer should be followed.

PET ACQUISITION AND PROCESSING PARAMETERS

The acquisition and processing parameters defined in this section apply to both the perfusion and metabolic PET tracers in the sections that follow.

Patient Positioning

Ideally, the patient should be placed in the supine position, with the arms out of the camera's FOV. Nearly all patients can tolerate this position, provided that some care is given to a method to support the arms. Alternatively, an overhead bar has often been used as a handhold for arm support. In patients with severe arthritis, whose arms cannot be positioned outside the camera's FOV, cardiac images should be obtained with the patient's arms resting on his/her side. In the latter case, the transmission scan time may have to be increased, and it is of critical importance that the arms not move between the transmission and emission scans, or artifacts will result. When performing perfusion/metabolism PET studies, it is imperative to keep the patient positioned similarly for both studies. In patients undergoing PET/CT imaging, arms resting inside the FOV will result in beam-hardening artifacts on the CT-based transmission scan, which usually lead to streak artifacts on the corrected emission scans.

Dose Considerations

In determining appropriate patient doses, the following issues should be considered:

1. Staff exposure could be high because of the limited effectiveness of shielding and the potential for large doses (e.g., ^{82}Rb PET). Thus, standing in close proximity to an ^{82}Rb generator or the patient during injection should be avoided. It is also important to point out that a lead apron is not helpful in shielding the 511-keV photons. In fact, it may increase staff

exposure due to secondary electrons emitted from the 511-keV photon interaction with lead.
2. Large patients may benefit from higher doses.
3. 3D imaging requires less dosage than 2D imaging due to the improved sensitivity of the system.

Total Counts

The counts per slice necessary to yield adequate quality images will vary from camera to camera depending, in part, on scatter and randoms corrections, as well as the amount of smoothing that is performed. If one tries to achieve on the order of 7 mm full width at half maximum (FWHM) in-plane resolution and has 10 to 15% scatter, then a typical good-quality study in 2D mode might have on the order of 50,000 true counts per millimeter of transaxial distance over the region of the heart (e.g., for a 4.25-mm slice separation, the number of counts would be $50{,}000 \times 4.25 = 250{,}000$ counts per slice). These numbers are approximate and may differ from one scanner to the other. If one is willing to accept a lower resolution (e.g., more smoothing) or more noise, imaging time can be reduced. 3D scanners have greater scatter, and therefore they usually require more counts than a 2D scanner to achieve the same noise level.

Pixel Size

It is recommended that 2–3 mm/pixel be used. A rule of thumb in nuclear medicine physics is that one should have at least 3 pixels for every FWHM of resolution in the image. For example, if the data are reconstructed to 8 mm FWHM, then this corresponds to roughly 8 mm/3 = 2.7 mm/pixel. Many institutions achieve a 3 mm sampling rate or better with a 256×256 array over the entire FOV of the camera. Other institutions choose to use a 128×128 array over a limited FOV (e.g., 25 to 35 cm diameter) centered over the heart, in which case, 2 to 3 mm/pixel is easy to achieve, cutting out extraneous structures in the FOV, even with a 128×128 array. Either method is acceptable to achieve the desired 2 to 3 mm/pixel. Greater than 3 mm/pixel may be acceptable for older PET cameras with resolution worse than 1 cm FWHM.

Imaging Mode (Static, Gated, or Dynamic)

Static PET acquisition produces images that allow relative assessment of tracer uptake on a regional basis. Comparison of regional tracer uptake in relation to the normal tracer distribution is the current standard for the identification of regional abnormalities. However, given the growing literature regarding the incremental value of absolute MBF measurement to the visual interpretation of relative radiotracer uptake, it is strongly recommended that the data be acquired in dynamic mode (i.e., binning the data with time).

Usually, PET tracer counts are sufficiently high to yield a good-quality ventricular function study. Electrocardiographic (ECG)-gated images are acquired in 8 to 16 time frames per R-to-R interval, in a manner similar to SPECT-gated perfusion studies but at higher spatial resolution. Given that ventricular contraction and thickening are often clinically useful for assessing viability, gating should be performed when possible. It is important that the gating software does not adversely affect the ungated images (e.g., by loss of counts as a result of beat length rejection). Monitoring the length and number of the accepted beats is critical to assure the accuracy of the gated data. Arrhythmias, such as atrial fibrillation, frequent premature ventricular contractions (PVCs), or other abnormal rhythms can lead to highly erroneous gated information. List-mode acquisition may obviate most of these problems.

For a dynamic acquisition, PET data are acquired in multiple time-sequenced frames. A potential advantage of the dynamic over static acquisition is patient motion artifact. For example, if a patient should move at the end of the study, select and utilize only those dynamic frames with no motion (i.e., summing them together to make one static image). This is easily implemented and takes almost no additional operator time. A more elaborate dynamic acquisition beginning just prior to the bolus injection of the tracer may be used optionally when kinetic analysis is to be performed (e.g., compartmental analysis or Patlak analysis). Kinetic analysis, which typically requires only the initial 3 to 5 minutes of data acquisition, permits absolute quantification of the tracer's kinetic properties (e.g., blood flow for ^{82}Rb and ^{13}N-ammonia, rate of ^{18}F-FDG utilization). Interpretation of quantitative MBF (or metabolic) data requires appropriate training and expertise beyond that necessary for visual inspection of static, summed images.

List-mode acquisitions are now available with nearly all cameras, which enable simultaneous dynamic and ECG-gated acquisitions. It is the optional acquisition mode, and is routinely used with many vendors' data processing software.

Image Reconstruction

Several corrections are required for creating datasets that can be used for reconstruction. PET data must be corrected for randoms, scatter, dead time, attenuation, and decay before reconstruction can begin. Once these corrections are applied, the data can be reconstructed with either filtered backprojection (FBP) or iterative

algorithms. FBP is the standard method used for reconstruction on older PET systems. FBP images are subject to streak artifacts, especially when the subject is obese or large. This can affect visual analysis but usually does not adversely affect quantitative analysis with regions of interest (i.e., the streaks tend to average out properly over typical volumes of interest). Newer PET systems employ iterative reconstruction methods (such as ordered subset expectation maximization [OSEM]) yielding images with superior noise properties. Although high-uptake structures, such as the heart, may not improve their noise characteristics with iterative reconstruction approaches, the surrounding lower uptake structures do improve, and streak artifacts are nearly eliminated, thus greatly improving the visual appearance of the image. However, low-uptake areas, such as myocardial defects and the left ventricular (LV) cavity at late times, may have slightly or artificially elevated activity levels unless sufficient iterations are performed. It is recommended that a cardiac phantom be used to characterize a PET machine and its reconstruction algorithm's behavior.

For rest/stress comparisons, the rest/stress images must have matched resolution. Filtering is usually necessary to achieve adequate noise properties. Care must be taken to match reconstructed resolution when making pixel-by-pixel comparisons of paired myocardial perfusion and metabolism data.

Attenuation Correction

Cardiac PET imaging should only be performed with attenuation correction. Attenuation correction can be accomplished with a rotating line source or ring in a dedicated PET system or with CT or MRI in a hybrid system.

For dedicated PET systems, two techniques are typically used for creating the patient-specific transmission scans: direct measurement of patient attenuation with a rotating line source of either ^{68}Ge or ^{137}Cs or segmentation of patient-specific attenuation maps. The former are very sensitive to the choice of reconstruction algorithm and, depending on the reconstruction algorithm used, could require 60 to 600 seconds acquisition time to produce a reasonable attenuation map. Segmentation algorithms are relatively insensitive to noise but are very dependent on the quality of the program used to perform the transmission scan segmentation and are influenced by lung-attenuation inhomogeneity (e.g., partial volume effects from the liver).

Transmission scans are typically acquired sequentially, so it is essential that the patient remains still between transmission and emission images. Either pre- or post-transmission scanning is acceptable, providing that the system's software can adequately correct for residual emission activity. Simultaneous acquisition of transmission and emission scans is not recommended unless the high count rate and rapidly changing distribution of the emission tracer can be assured to not adversely affect the transmission scan. If the transmission scan is performed at the beginning of the study, attention should be made for potential misregistration with the emission scans, possibly due to gradual upward creep of the diaphragm, due to pressure from visceral fat.[21]

For PET/CT or PET/MR systems, CT or MR can be used for acquiring a transmission scan for attenuation correction. An advantage of this approach is the rapid acquisition of the transmission scan, which can be repeated for each imaging session, rest and stress perfusion studies, as well as for subsequent metabolic imaging, if necessary. The CT or MR scan can be reviewed for additional, independent diagnostic information, such as coronary calcium visualization and other extra-cardiac anatomic information. To acquire a CT- or MR-based transmission scan, it is necessary to first acquire a planar scout acquisition. This scan is used to measure the axial limits of the full acquisition. Following this acquisition, the transmission scan is acquired. The best approach for CT transmission scanning is still evolving, and therefore this guideline can only suggest some considerations. Some of the considerations for CT scanning are as follows (see Table 5):

1. If CT is used for either attenuation correction or anatomical evaluation, it will have an effect on the kVp and mAs used in the acquisition. A transmission scan usually requires only a low CT current, as opposed to calcium scoring or CT angiography, which require higher CT currents.
2. Breathing protocols are not fully established. Recent data suggest that respiratory averaging may be a useful method of reducing breathing-related artifacts. Other methods, such as free breathing with a slow CT scan or ultra-rapid CT acquisition (depending on the CT device available), have also been proposed. Current practice discourages breath holding, particularly in end-inspiration because of the potential for it to cause uncorrectable misregistration. A CT transmission scan performed at the same speed, as for whole-body PET/CT images, frequently produces artifacts at the lung-liver interface and can sample parts of the heart and diaphragm in different positions, causing misregistration and an artifact where pieces of the diaphragm appear to be suspended in the lung. Although specifics vary among laboratories, the duration of the CT transmission scan is typically from 10 to 30 seconds. CT attenuation correction with 64-slice devices can achieve an ultra-rapid CT scan in 1.5 seconds, which appears to reduce such CT artifacts. Therefore, it is imperative

Table 5. General guidelines for CT-based transmission PET imaging

CT parameter	General principle	Effect on patient dose
Slice collimation	Should approximate the slide thickness of PET (e.g. 4-5 mm)	No effect
Gantry rotation speed	Slower rotation speed helps blur cardiac motion (e.g. 1 sec/revolution of slower	Slower gantry rotation increase radiation dose
Table feed per gantry rotation (pitch)	Relatively high pitch (e.g. 1:1)	Inversely related to pitch
ECG gating	ECG gating is not recommended	Decreases without ECG gating
Tube potential	80-140 kVp, depending on manufacturer specification	Increases with higher kVp
Tube current	Because the scan is only acquire for AC, low tube current is preferred (10-20 mA)	Increases with higher mA
Breathing instructions	End-expiration breathhold or shallow free-breathing is preferred	No effect
Reconstruction slice thickness	Should approximate the slice thickness of PET (e.g. 4-5 mm)	No effect

to ensure proper registration between transmission and emission scans for quality assurance and proper interpretation of PET images. Several approaches are currently being devised to reduce misregistration artifacts, such as reducing CT tube current and increasing the duration CT acquisition to better match the temporal resolution between the attenuation and emission maps.[22,23]

3. Metal artifacts can present a challenge for the reconstruction algorithm and must be compensated for to produce accurate attenuation maps.[24,25]

Although pacemaker leads do not appear to cause artifacts in cardiac PET/CT images, automatic implantable cardioverter defibrillator leads frequently do result in artifacts of sufficient magnitude to impact clinical image interpretation.[24] Ideally, stress transmission scans should be acquired during peak stress or vasodilation, although this is not practical.

As such, the technologist and physician must carefully inspect the transmission and emission image sets to ensure that they are properly registered in the transaxial, sagittal, and coronal planes. For patients undergoing PET/CT, a separate, CT-based transmission scan for correction of the stress images is standard. For ^{82}Rb, a post-stress transmission scan is preferred to minimize misregistration artifacts on the corrected ^{82}Rb images when misregistration compensation software is not available.

PET MYOCARDIAL PERFUSION IMAGING

PET MPI is an important diagnostic and prognostic technique in the assessment of patients with known or suspected CAD. The goal of evaluating myocardial perfusion with PET imaging is to detect physiologically significant coronary artery narrowing to guide clinical management of patients with known or suspected CAD and those without overt CAD but with cardiovascular risk factors in order to:

- evaluate the progression of atherosclerosis,
- determine cause of ischemic symptoms and recommend medical or revascularization therapy,
- estimate the potential for future adverse events, and
- improve patient survival.

Stress and rest paired myocardial perfusion studies are commonly performed to assess myocardial ischemia and/or infarction. Current Food and Drug Administration (FDA)-approved and CMS-reimbursable PET MBF tracers are limited to ^{82}Rb and ^{13}N-ammonia. While ^{15}O-water is also used clinically in Europe, it is not FDA approved in the United States. There are also ^{18}F-labeled MBF agents that are currently investigational and in clinical trials.

Normal myocardial perfusion on stress images implies the absence of physiologically significant CAD. Abnormal myocardial perfusion on stress images suggests the presence of significantly narrowed coronary arteries. However, it is important to point out that such visual interpretation of relative radiotracer uptake may underestimate balanced reduction in blood flow in all three vascular territories, also termed ‘‘balanced ischemia.’’ Routine assessment of absolute quantitative MBF may identify such patients as well as those with equivocal or borderline radiotracer uptake defects. If the stress-induced regional perfusion defect persists on the corresponding paired rest images, it suggests the

presence of an irreversible myocardial injury. On the other hand, if the defect on the stress images resolves completely or partially on the rest images, it suggests the presence of stress-induced myocardial ischemia. Absolute quantitative MBF may provide further insight into coronary steal phenomenon, defined as an absolute decrease in vasodilator stress perfusion from resting blood flow in collateral-dependent myocardium as well as in hibernation. Low resting MBF may or may not increase with stress but is nonetheless viable requiring an assessment of myocardial metabolism. In the case of hibernation, imaging of myocardial perfusion can be combined with myocardial metabolism imaging with ^{18}F-FDG for the assessment of myocardial viability in areas of resting hypoperfusion and dysfunctional myocardium.

Patient Preparation

Patient preparation is similar to preparation for stress and rest myocardial perfusion SPECT imaging. This includes fasting for 6 hours or more, with the exception of water intake. Patients should avoid caffeinated beverages for at least 12 hours, and avoid theophylline-containing medications for at least 48 hours.[26]

Cardiac Stress Testing

Details of pharmacologic or exercise stress testing are beyond the goals of this document. Nonetheless, stress protocols are, for the most part, generic for all perfusion agents.[26] The specific differences in acquisition protocols for ^{82}Rb and ^{13}N-ammonia imaging are related to the duration of uptake and clearance of these radiopharmaceuticals, their physical half-lives, and the characteristics of the vasodilators used for the study. For example, the time course of action of the A_{2A}-selective adenosine receptor agonist, regadenoson, is longer than that of adenosine (peak-effect onset at $\sim$1 min post bolus injection with a duration of approximately 8 to 10 minutes at $\geq$80% peak effect).[27] As such, accurate quantification of MBF is critically dependent on the interplay between the vasodilator and the timing of the radiotracer injection in relation to the peak coronary vasodilation achieved by the drug.[28–31] In addition, all contraindications for performing cardiac stress testing with SPECT also apply to PET.[31]

^{82}Rb Perfusion Imaging

Tracer properties. ^{82}Rb PET MPI is a well-established and highly accurate technique for the diagnosis of hemodynamic CAD.[32–34] ^{82}Rb is a monovalent cationic analog of potassium. It is produced in a commercially available generator by decay from ^{82}Sr attached to an elution column. ^{82}Sr has a half-life of 25.5 days and decays to ^{82}Rb by electron capture. ^{82}Rb decays with a physical half-life of 75 seconds by emission of several possible very high-energy positrons. The resulting long positron range worsens image resolution compared to ^{18}F and ^{13}N. The daughter product is krypton-82, which is stable. The ^{82}Sr-containing generator is commercially available and is replaced every 6 weeks, thus obviating the need for a cyclotron.

^{82}Rb is eluted from the generator with 10 to 50 mL of normal saline by a computer-controlled elution pump, connected by intravenous (IV) tubing to the patient. The generator is fully replenished every 10 minutes. While the short half-life of ^{82}Rb challenges the performance limits of PET scanners, it facilitates the rapid completion of a series of rest and stress myocardial perfusion studies.

^{82}Rb is extracted from plasma with high efficiency by myocardial cells via the Na/K adenosine triphosphatase pump. Its first-pass extraction is considerably less than that of ^{13}N-ammonia, and decreases rapidly with increasing blood flow. ^{82}Rb extraction can be decreased by severe acidosis, hypoxia, and ischemia.[35–37] Thus, while uptake of ^{82}Rb predominantly depends on MBF, it may be modulated by metabolism and cell membrane integrity.

Dosimetry. The radiation dosimetry from ^{82}Rb in an adult may vary from 1.1 to 3.5 mSv total effective dose for a maximal allowable activity of 60 mCi injection for each rest and stress study.[38,39] With current advances in PET instrumentation, diagnostic quality PET images can be acquired using only 20 to 40 mCi of ^{82}Rb for each of the rest and stress images of the study resulting in lower radiation exposure.

Scout scanning. Scout scanning is recommended before each injection to ensure that the patient is correctly positioned and is not exposed to unnecessary radiation. This can be done with a fast transmission scan or with a low-dose ^{82}Rb injection (10 to 20 mCi). The low-dose ^{82}Rb scout scan is also used to estimate circulation times and cardiac blood pool clearance times, which assist in selection of the optimum injection-to-imaging delay time between ^{82}Rb injection and initiation of acquisition of myocardial ^{82}Rb images. However, given the growing literature regarding the incremental value of absolute MBF measurement to the visual interpretation of relative radiotracer uptake, it is strongly recommended that the default acquisition be set at dynamic list mode, thereby allowing the user to have the option of interpreting visual and/or quantitative data. With PET/CT systems, a low-dose x-ray scout scan is routinely used for patient positioning.

Imaging parameters. Rest imaging should be performed before stress imaging to reduce the impact of

residual stress effects (e.g., stunning and steal). For ^{82}Rb, about 80% of the useful counts are acquired in the first 3 minutes, 95% of the useful counts are obtained in the first 5 minutes, and 97% are obtained in the first 6 minutes. The patient should be infused with ^{82}Rb for a maximum of 30 seconds. After the dose is delivered, patients with normal ventricular function, or left ventricular ejection fraction (LVEF) >50%, are typically imaged starting 70 to 90 seconds after the injection. For those with reduced ventricular function, or LVEF from 30 to 50%, imaging usually is begun 90 to 110 seconds after termination of the infusion. Those with poor function, or LVEF <30%, are typically imaged at 110 to 130 seconds. Excessive blood pool counts can scatter into myocardial counts, impacting defect size and severity (Tables 6 and 7).

^{13}N-Ammonia Perfusion Imaging

^{13}N-ammonia is a valuable agent for measuring either absolute or relative MBF.[40,41] For measurements of absolute MBF, dynamic acquisition from time of injection is required, followed by applying 2- and 3-compartment kinetic models that incorporate both extraction and retention rate constants. In a clinical setting, ^{13}N-ammonia PET myocardial perfusion images are assessed visually or semiquantitatively along with absolute MBF measurements with commercially available software for the evaluation of regional myocardial perfusion defects.[42–46]

^{13}N-ammonia is an extractable myocardial perfusion tracer that has been used extensively in scientific investigations with PET for more than three decades. At physiologic pH, ^{13}N-ammonia is in its cationic form with a physical half-life of 10 minutes. Its relatively short half-life requires an on-site cyclotron and radiochemistry synthesis capability. ^{13}N decays by positron emission. The daughter product is carbon-13, which is stable. Myocardial uptake of ^{13}N-ammonia depends on flow, extraction, and retention. First-pass myocardial extraction of ^{13}N-ammonia is related inversely and nonlinearly to blood flow[47] Following this initial extraction

Table 6. ^{82}Rb rest/stress myocardial perfusion imaging guideline for BGO and LSO (LYSO) PET imaging systems

Feature	BGO Systems	LSO (LYSO) Systems	Technique
Stress testing	Pharmacologic agents		Standard
Tracer dose			
2D scanner	40-60 mCi (1480-2220 MBq)		Standard
3D scanner	10-20 mCi (370-740 MBq)	30-40 mCi (1110-1480 MBq)	Standard
Injection rate	Bolus of ≤30 seconds		Standard
Imaging delay after injection	LVEF >50%: 70-90 seconds LVEF <50% or unknown: 90-130 seconds List mode: acquire immediately		Acceptable
Patient positioning			
PET	Use scout scan: 10-20 mCi (370-740 MBq) ^{82}Rb		Standard
	Use transmission scan		Optional
PET/CT	CT scout		Standard
Imaging mode	List mode: gated/dynamic (no delay after injection)		Preferred
	Gated acquisition (delay after injection		Optional
Imaging duration	3-6 minutes		Standard
	3-10 minutes		Optional
Attenuation correction	Measure attenuation correction, before or after		Standard
Reconstruction method	FBP or iterative expectation maximization (e.g. OSEM)		Standard
Reconstruction filter	Sufficient to achieve desired resolution/smoothing, matched stress to rest		Standard
Reconstructed pixel size	2-3 mm		Preferred

Table 7. ^{82}Rb rest/stress myocardial perfusion imaging guideline for GSO PET imaging systems

Feature	GSO Systems	Technique
Stress testing	Pharmacologic agents	Standard
Tracer dose (3D)	20 mCi (740 MBq)	Standard
Injection rate	Bolus of ≤30 seconds	Standard
Imaging delay after injection	LVEF >50%: 70-90 seconds LVEF <50% or unknown: 90-130 seconds List mode: acquire immediately Longer delays than the above must be used if count rate at these times exceeds the maximum value specified by the manufacturer	Standard
Patient positioning PET PET/CT	 Use scout scan: 10-20 mCi (370-740 MBq) ^{82}Rb Use transmission scan CT scout	 Standard Optional Standard
Imaging mode	List mode: gated/dynamic (no delay after injection)	Standard
Imaging duration	3-6 minutes 3-10 minutes	Standard Optional
Attenuation correction	Measure attenuation correction, before or after	Standard
Reconstruction method	Iterative row-action maximum likelihood algorithm (3D-RAMLA)	Standard
Reconstruction filter	None	Standard
Reconstructed pixel size	4 mm	Standard

across the capillary membrane, ^{13}N-ammonia may cross myocardial cell membranes by passive diffusion or as an ammonium ion by the active sodium-potassium transport mechanism. Once in the myocyte, ^{13}N-ammonia is either incorporated into the amino acid pool as ^{13}N-glutamine or back-diffuses into the blood. The myocardial tissue retention of ammonia as ^{13}N-glutamine is mediated by adenosine triphosphate and glutamine synthetase. Thus, uptake and retention can both be altered by changes in the metabolic state of the myocardium, although the magnitude of metabolic effects on the radiotracer retention appears to be small.

Dosimetry. The radiation dosimetry from a 20 mCi dose of ^{13}N-ammonia is 1.48 mSv total effective dose in an adult.[48] The critical organ is the urinary bladder, which receives 6 mSv from a 20 mCi dose of ^{13}N-ammonia.[48] The dosimetry is relatively low, due to the short half-life of ^{13}N and the low energy of the emitted positrons.

Acquisition parameters. Table 8 summarizes the recommended guidelines for performing ^{13}N-ammonia perfusion scans with dedicated, multicrystal PET or PET/CT cameras for rest and stress PET MPI for the diagnosis and evaluation of CAD, or as part of an assessment of myocardial viability.

Dose. Typically, 10 to 20 mCi of ^{13}N-ammonia is injected. Large patients may benefit from higher, 25 to 30 mCi, doses. In addition, the dose of radioactivity administered will also depend on whether images are obtained in 2D or 3D imaging mode.

Non-FDA-Approved Myocardial Perfusion Agents

^{15}O-water is often considered the ideal radiotracer for quantifying MBF in absolute terms.[49–53] Because the capillary and sarcolemmal membranes do not exert a barrier effect on the exchange of water, the activity of ^{15}O-labeled water observed in an assigned region of interest to the myocardium on the serially acquired images can be described by a one-compartment tracer kinetic model. ^{15}O-water is not FDA approved, and therefore it is not used clinically in the United States. It is, however, used in Europe for clinical imaging. Initial studies with ^{18}F-labeled MBF agent, flurpiridaz, in humans has shown a very good diagnostic accuracy for the detection of significant CAD.[34] Regarding its potential for quantification of absolute MBF, in an experimental study, measurement of the standardized uptake value (SUV) obtained at 5 to 10 minutes after

Table 8. ^{13}N-ammonia cardiac PET perfusion studies

Feature	Acquisition parameters	Technique
Stress testing	Pharmacologic agents	Standard
Tracer dose (2D or 3D)	10-20 mCi (370-740 MBq) typical	Standard
Injection rate	Over 20-30 second infusion	Preferred
Imaging delay for static images	1.5-3 minutes after end of infusion	
Imaging delay for dynamic images	Start camera prior to dose infusion	Preferred
Patient positioning PET PET/CT	 Use scout scan: 1-2 mCi (37-74 MBq) Use transmission scan CT scout	 Optional Standard Standard
Imaging mode	ECG gating of myocardium Static List mode: gated/dynamic	Preferred Optional Preferred
Imaging duration	10-15 minutes	Standard
Attenuation correction	Measure attenuation correction, before or after	Standard
Reconstruction method	FBP or iterative expectation maximization (e.g. OSEM)	Standard
Reconstruction filter	Sufficient to achieve desired resolution/smoothing, matched stress to rest	Standard
Reconstructed pixel size	2-3 mm 4 mm	Preferred Optional

^{18}F-flurpiridaz IV injection showed a linear correlation with adenosine hyperemia MBF as quantified by radio-labeled microspheres.[54]

IMAGE DISPLAY, NORMALIZATION, AND EVALUATION FOR TECHNICAL ERRORS

Recommendations for display of PET perfusion rest-stress and/or perfusion/metabolism images are consistent with those listed in previous guidelines for rest-stress SPECT MPI.[55] It is necessary to examine the transaxial, coronal, and sagittal views for assessing the alignment of the emission images acquired during stress, rest, and metabolism, as well as the transmission images. Fused transmission and emission images are preferred. Images that are not aligned (e.g., due to patient or cardiac motion) may cause serious image artifacts, especially when only one set of attenuation correction images has been applied to all emission images for attenuation correction. This is a problem particularly when CT is used for attenuation correction.[19] It is important that the fusion images be reviewed for potential misalignment problems and appropriate adjustments are made. Some vendors' systems now provide software that allows realignment of transmission CT and emission PET images before processing, and in other instances image data can be transferred to a standalone PC that has realignment software.

The reoriented images should be displayed as follows:

1. A short-axis view, by slicing perpendicular to the long axis of the LV from apex (left) to base,
2. A vertical long-axis view, by slicing vertically from septum (left) to lateral wall, and
3. A horizontal long-axis view, by slicing from the inferior (left) to the anterior wall.

For interpretation and comparison of perfusion and metabolism images, slices of all datasets should be displayed aligned and adjacent to each other. In the absence of motion artifact, combined assessment of perfusion and metabolism within a single PET session offers the advantage of copying the ventricular long axis defined during image orientation from one image set to the second set, thereby optimizing the matching of the perfusion with the metabolism images. Normalization of the stress and rest perfusion image set is commonly performed using the maximal myocardial pixel value in each of the two or three image sets, or, for example, the average pixel value with the highest 5% of activity of the perfusion images. Each perfusion study is then normalized to its own maximum.

The metabolism images are normalized to the counts in the same myocardial region on the resting perfusion images (e.g., with the highest count rates that were obtained on the perfusion study).[56,57] An important limitation of this approach, however, is that glucose metabolism may be enhanced or abnormally increased in regions with apparently normal resting myocardial perfusion, if such regions are subtended by significantly narrowed coronary arteries and are in fact ischemic on stress myocardial perfusion studies.[58] Moreover, visual assessment of resting myocardial uptake of the radiotracer reflects the distribution of MBF in ''relative'' terms (i.e., relative to their regions of the LV myocardium) and not in ''absolute'' terms (i.e., mL/min/gm myocardial tissue). Thus, in some patients with multivessel CAD, it is possible that all myocardial regions are in fact hypoperfused at rest in ''absolute'' terms (i.e., characterized as balanced reduction in blood flow) and yet appear normal in ''relative'' terms. Quantitative resting MBF may be used to define the region with the highest absolute MBF for normalization of the metabolism data. Whether absolute quantification of regional myocardial glucose utilization may also aid in this distinction is not well established in the literature. If stress myocardial perfusion PET images are available, it is recommended that the normal reference region on stress perfusion images be utilized.[40] In the presence of left bundle branch block (LBBB), where the septal ^{18}F-FDG uptake is spuriously decreased, the septum should not be used as the site for normalization. Accordingly, the ECG should be reviewed in conjunction with perfusion/viability imaging.

Standard Segmentation and Polar Map Display

The standard segmentation model divides the LV into three major short-axis slices: apical, mid-cavity, and basal. The apical short-axis slice is divided into four segments, whereas the mid-cavity and basal slices are divided into six segments. The apex is analyzed separately, usually from a vertical long-axis slice. Although the anatomy of coronary arteries may vary in individual patients, the anterior, septal, and apical segments are usually ascribed to the left anterior descending coronary artery, the inferior and basal septal segments to the right coronary artery, and the lateral segments to the left circumflex coronary artery. The apex can also be supplied by the right coronary and left circumflex artery. Data from the individual short-axis tomograms can be combined to create a polar map display, representing a 2D compilation of all the 3D short-axis perfusion data. The 2D compilation of perfusion and metabolism data can then easily be assigned to specific vascular territories. These derivative polar maps should not be considered a substitute for the examination of the standard short-axis and long-axis cardiac tomographic slices.

3D Display

If suitable software is available, reconstructed myocardial perfusion and metabolism datasets can be displayed in a 3D static or cine mode, which may be convenient for morphologic correlation with angiographic correlation derived from CT, MR, or conventional angiography. Some of the software may allow the overlay of the coronary anatomy on the 3D reconstructed perfusion and metabolism images of the heart. An advantage of 3D over conventional 2D displays with regard to accuracy of PET image interpretation has not been demonstrated.

Recommended Medium for Display

It is strongly recommended for the interpreting physician to use the computer monitor rather than film hard copies for interpretation of myocardial perfusion and metabolism images. The latter would be especially important for gated PET images, where dynamic wall motion data are viewed for proper interpretation of regional abnormalities. A linear gray scale, monochromatic color scale, or multicolor scale can be used as the type of display, depending on user experience and preference.

Image Evaluation for Technical Sources of Errors

Patient motion. PET images are typically generated with non-moving circular arrays of scintillation detectors that acquire all projection data simultaneously. In contrast, SPECT imaging with rotating gamma cameras—in which patient motion leads to a typical misalignment between adjacent projection images—can be identified by viewing a projection movie. Movement during static PET imaging affects all projections and is therefore more difficult to identify. Substantial patient motion can produce blurring of image contours. Therefore, attention to patient motion during image acquisition is essential to minimize motion artifacts.

Patient positioning before and immediately after image acquisition should be carefully evaluated (e.g., by checking the alignment of the camera's positioning laser beams with ink markers on the patient's skin). Acquisition of a scout scan after injection of a small dose, usually one-third of the standard dose of ^{82}Rb, may facilitate accurate patient positioning. With PET/CT systems, a low-dose x-ray scout scan (10 mA) is

routinely used for accurate patient positioning. In instances of patient discomfort and likely patient motion, especially during longer image acquisition times, one approach to reduce the potential for motion artifacts is to acquire a series of 3 to 4 sequential image frames instead of a single static image of longer duration. Dynamic imaging would also be effective for this purpose. If the quality of one of the serially acquired frames is compromised by motion, then that frame can be rejected and only frames that are of acceptable quality and are free of motion artifacts are summed for the final image analysis.

Vertical and transaxial displacement of the heart can occur even in the absence of chest movement. The latter is perhaps related to the change of breathing pattern, which may occur during pharmacologic stress. This could be thought of as analogous to the ''upward creep'' phenomenon seen in SPECT imaging. As a result, under-correction artifacts due to the lower attenuation coefficient of the overlapping lung tissue may appear in the anterior or anterolateral regions, or over-correction artifacts due to the higher attenuation coefficients of the overlapping subdiaphragmatic tissues may appear in the inferior region as hot spots. Inspection of fused emission-transmission images for possible misalignment is essential because the resulting artifacts would greatly affect image interpretation. Fused images should be inspected in the axial (lateral displacement), coronal (vertical displacement), and sagittal (vertical displacement) slices. Alternatively, displacement can be detected on transaxial images by counting the number of pixels by which the cardiac image is displaced between resting-and-stress transaxial acquisitions. Identification of vertical and lateral displacements that result in misalignment between the emission and transmission images is relatively straightforward.

The degree of co-registration of transmission and emission images should be carefully examined using the fusion software available on integrated PET/CT systems to assess the reliability of images with attenuation correction. If there is patient motion, the cardiac silhouette may not superimpose perfectly on the transmission and emission images. If the transmission or emission scans are degraded by motion during the acquisition, software may not correct the image quality and the scan may have to be repeated. In general, vertical misalignment is easier to resolve by offsetting the alignment between the emission and transmission scans, but this option is not generally available. When the transmission scans are acquired using CT, the incidental findings in the portion of the chest in the FOV should be reported, when relevant to patient care.

Reconstruction artifacts. Image artifacts may occur if extra-cardiac activity is present, adjacent to the myocardium. For example, intense focal activity in the liver or the gastrointestinal tract may lead to spillover of residual activity from imperfect scatter compensation, resulting in artificially elevated counts, or cause a reconstruction (i.e., ramp filter) artifact resulting in apparent low count rates in adjacent myocardium. While these artifacts are common in SPECT imaging, they are rare in PET imaging. Additional artifacts can result from problems with CT transmission images, such as streaks caused by insufficient x-ray tube intensity in obese individuals, truncations, beam hardening resulting from bone (e.g., arms down) or metal adjacent to the heart (e.g., pacemakers and internal defibrillators), and breathing leading to disconnected pieces of liver in the lungs or misalignment between CT and PET data. CT artifacts are propagated into the PET images through the use of CT image for attenuation and scatter corrections. These artifacts are less of a problem with ^{137}Cs attenuation correction.

Image count statistics. The final count density of PET images is influenced by additional factors, such as body habitus and weight, radionuclide dose, scanner performance, acquisition time, and in the case of metabolic imaging, the dietary and neurohormonal state of the patient. Image count density directly affects the diagnostic quality and reliability of the study.

Image Analysis and Interpretation of PET Images

The rest and stress perfusion and/or metabolism images should be interpreted initially without clinical information in order to minimize any bias in study interpretation. All relevant clinical data should be reviewed after a preliminary impression is formed.

LV and RV size. The reader should note whether there is an enlargement of the right ventricle (RV) or LV at rest or whether there is transient stress-induced LV cavity dilatation. Ventricular enlargement seen on the stress and rest perfusion or metabolic images generally indicates left, right, or bi-ventricular dysfunction. LV and RV sizes, as well as any changes associated with stress, are typically described qualitatively. A number of commercially developed software packages originally developed for SPECT have the ability to quantify mean LV volumes and end-diastolic and end-systolic volumes for gated PET images, but not all such packages have been validated for all PET instruments. Among other considerations, PET stress images are acquired at the peak of pharmacologic stress, as opposed to SPECT for which images are acquired 15 to 45 minutes after stress.

Lung uptake. Increased tracer activity in the lungs should be reported qualitatively. Increased lung uptake on the perfusion images, particularly when

severe, may reflect severe LV dysfunction with increased LV end-diastolic and capillary wedge pressures. It can also reflect infiltrative diseases of the lungs, and can be seen in smokers. Increased lung uptake can adversely affect image quality, and in particular may interfere with interpretation of the lateral wall. It may be necessary to increase the time between injection and image acquisition from 4-5 minutes to 7-8 minutes.[59,60]

RV uptake. Increased RV tracer uptake may be seen both on perfusion and metabolism images in the presence of pulmonary hypertension with or without significant RV hypertrophy. Increased RV uptake is usually assessed relative to the radiotracer uptake in the LV myocardium. Because the septum is shared by both ventricles, assessment of increased RV uptake should be made in relation to other regions of the LV myocardium. Abnormally increased RV tracer uptake is a qualitative assessment. When RV uptake relative to the LV is increased at stress compared to rest, this may indicate three-vessel or left main disease and balanced ischemia (indicating a relative reduction in LV perfusion rather than increased RV perfusion).[61]

Blood pool activity. Visualization of persistent blood pool activity on either perfusion or metabolism images is usually a sign of relatively poor myocardial uptake of the radiotracer, insufficient time for uptake of the radiotracer into the myocardium, or diminished clearance of the radiotracer from blood. A major cause of increased blood pool activity, especially for perfusion imaging with ^{82}Rb, is impairment of cardiac systolic function that prolongs the circulation time. This is especially relevant when only static images are acquired, because vasodilators typically increase cardiac output and shorten the circulation time. List-mode acquisition allows for the reprocessing of images with varying delay times and may be useful for optimizing the quality of reconstructed images.

Extra-cardiac findings. The tomographic images should be carefully examined for uptake of the radiotracer in organs other than the myocardium, particularly in the lungs and the mediastinum. Extra-cardiac uptake of a flow tracer may be of clinical significance, as it may be associated with malignancy and/or an inflammatory process. The 3D maximum intensity projection display, a method of displaying acquired PET images as a rotating 3D display, can be particularly helpful in this regard. When using PET/CT systems, review of the low-resolution CT-based transmission image can be useful to delineate potentially important ancillary findings, such as pleural and pericardial effusion, coronary and/or aortic calcification, breast, mediastinal, or lung mass, and others.

Normal variants. Apparent persistent reduction of activity at stress and rest can be seen at the apex on PET perfusion images and is a normal variant related to a partial volume artifact due to apical thinning relative to the remainder of the myocardium. This may be seen with ^{82}Rb or ^{13}N ammonia—often more evident with ^{13}N-ammonia and with TOF cameras. Persistent reduction at stress and rest in the lateral wall is a common variant in ^{13}N-ammonia imaging, more evident in a normal-sized and functioning ventricle. The precise explanation of this finding has been elusive but appears to be unique to ^{13}N-ammonia and may relate to differences in retention or wall motion of the lateral wall versus the septum.[62]

Interpretation of PET Perfusion Data

Perfusion defect location, severity, and extent. Myocardial perfusion defects should be identified through careful visual analysis of the reoriented myocardial slices. Perfusion defects should be characterized by extent, severity, and location relative to the specific myocardial territory, such as the anterior, lateral, inferior, septal, and/or apical walls. Standardized nomenclature should be used, according to previously published guidelines.[63] RV defects due to scarring and ischemia should be noted.

Qualitative scoring. Defect extent should be qualitatively estimated by describing the location of the abnormal segments involved (e.g., anterior, inferior, or lateral) as well as the extent in the LV (e.g., 'mid-to-distal' or 'extending from base to the apex'). The extent of the defect may also be qualitatively described as small (5 to 10% of the LV), medium (10 to 20% of the LV), or large (20% of the LV). A defect of more than 10% of the LV is associated with a higher risk of cardiac events. Defect severity is typically expressed qualitatively as mild, moderate, or severe. Severe defects may be considered as those having a tracer concentration equal or similar to background activity, and moderate defects are considered definitely abnormal but visually discernable activity above the background. Mild defects are those with a subtle but definite reduction in regional myocardial tracer uptake.

Stress and rest myocardial perfusion image sets are compared in order to determine the presence, extent, and severity of stress-induced perfusion defects and to determine whether such defects represent regions of myocardial ischemia or infarction. Regions with stress-induced perfusion abnormalities, which have normal perfusion at rest, are termed reversible perfusion defects and represent ischemia. Perfusion abnormalities on stress, which remain unchanged on rest images, are termed irreversible or fixed defects, and most often represent areas of prior myocardial infarction. When both ischemia and scar are present, the defect

Table 9. Semiquantitative scoring system of defect severity and extent

Grade	Interpretation	Score
Normal counts	Normal perfusion	0
Mild reduction in counts	Mildly abnormal	1
Moderate reduction in counts	Definitely abnormal	2
Severe reduction in counts	Definitely abnormal	3
Absent counts	Definitely abnormal	4

reversibility is incomplete, giving the appearance of partial reversibility.

Semiquantitative scoring system. In addition to the qualitative assessment of perfusion defects, a well-accepted 5-point scale semiquantitative visual scoring method is used in direct proportion to the observed count density of the segment, as follows: 0 = no defect; 1 = mildly reduced; 2 = moderately reduced; 3 = severely reduced; 4 = absent activity (Table 9). This approach standardizes the visual interpretation of scans, reduces the likelihood of overlooking clinically significant defects, and provides a semiquantitative index that is applicable to diagnostic and prognostic assessments.

A 17-segment model for semiquantitative visual analysis can also be employed.[63] The model is based on three short-axis slices (apical, mid, and basal) to represent most of the LV and one vertical long-axis slice to better represent the LV apex (Figure 1). The basal and mid-short-axis slices are divided into six segments. The apical short-axis slice is divided into four segments. A single apical segment is taken from the vertical long-axis slice. Each segment has a specific name. The extent of stress and rest perfusion abnormalities, as well as an estimate of the extent of scarring and ischemia, can be performed by counting the number of segments.

Myocardial segments may be assigned to coronary artery territories. Caution should be exercised because the coronary anatomy varies widely among patients. For example, it is not uncommon to find segments 9, 10, and 15 (of the 17-segment model) involved in left anterior descending artery disease. Similarly, segments 5 and 11 of the model may be affected by disease of the right coronary artery.

Degree of abnormality by % myocardium stress (17-segment model)	
Normal	SSS = 0-3 (<5% myocardium)
Mildly abnormal	SSS = 4-7 (5%-10% myocardium)
Moderately or severely abnormal	SSS > 8 (>10% myocardium)

In addition to individual scores, calculation of summed scores is recommended, in which the summed stress score (SSS) is the sum of the stress scores of all segments, the summed rest score (SRS) is the sum of the resting scores of all segments, and the summed difference score (SDS) is the difference between the summed stress and summed rest scores and serves as a measure of reversibility. The summed scores incorporate the global extent and severity of perfusion abnormality. For example, the SSS reflects the extent and severity of perfusion defects at stress and is affected by prior myocardial infarction as well as by stress-induced ischemia.

On the other hand, the SRS reflects the amount of infarcted and/or hibernating myocardium. The SDS is a measure of the extent and severity of stress-induced ischemia.

Before scoring, it is necessary for the interpreting physician to be familiar with the normal regional variation in count distribution of myocardial perfusion PET. No regional variation in tracer uptake has been reported for ^{82}Rb, except for a mild reduction in the apex and base of the LV, consistent with segmentation artifact and/or thinning of the LV myocardium in these locations. Regarding ^{13}N-ammonia, unlike ^{82}Rb and other SPECT perfusion tracers, the lateral wall uptake may not necessarily be the region with the highest counts, serving as the reference region for normalization. This normal variation should be kept in mind when visually interpreting lateral perfusion defects with ^{13}N-ammonia PET.[62] Absolute quantitative MBF of the lateral wall has been shown to further differentiate a true perfusion defect from normal variant in the clinical setting. In addition, apical thinning may be more pronounced with TOF ^{13}N-ammonia imaging. Given the variability in the normal distribution of various radiotracers, the patient's polar map may be compared with a reference polar map derived from radiotracer and gender-specific normal database. Ideally, each camera system and acquisition protocol should have its own ''normal'' file but such normal databases are not widely available. The semiquantitative analysis system provided by a specific vendor should be validated by appropriate studies published in peer-reviewed journals.

Absolute quantification of myocardial blood flow. Quantitative blood flow approaches offer an objective interpretation that is inherently more reproducible than visual analysis.[64–66] Absolute quantification may aid in assessing the physiologic significance of known coronary artery stenosis, especially when of intermediate severity. Both relative and absolute quantification are particularly useful in describing changes between two studies in the same patient. In addition, quantitative measurements of MBF may identify balanced reductions in MBF due to balanced multivessel CAD or diffuse small-vessel disease.

Software packages that are commonly used for quantitative analysis of SPECT perfusion images have been developed for PET.[67] These analyses portray relative uptake of tracer in reference to limits derived from PET images (^{82}Rb or ^{13}N-ammonia) of patients with a low likelihood of coronary disease, but do not present true blood flow quantitation values. High diagnostic accuracy for detecting obstructive CAD has been reported.[68,69] Similar to SPECT, PET total perfusion deficit values for stress, rest, and defect reversibility (i.e., ischemia) can be derived, but use of these parameters to guide patient management has not been established. The various analytic software packages also provide quantitative data for LV volumes and ejection fractions. As is the case with SPECT, it must be recognized that different packages do not provide the same values, something that must be understood when deciding whether a finding is normal or abnormal, as well as when repeat images are done for a patient using different analytic software.[70]

Quantitative absolute hyperemic MBF in mL/min/gm tissue and flow reserve (representing the ratio of hyperemic and resting MBF)—derived from dynamic acquisition with measurements of resultant myocardial and blood pool time-activity curves—is a potentially powerful adjunct to PET perfusion imaging. It is important to recognize, however, that myocardial flow reserve (MFR) ratio can be spuriously lowered by elevated resting blood flow in the denominator, as seen in patients with hypertension or high resting rate-pressure product. Thus, it is important to interpret both hyperemic MBF and flow reserve in all subjects. Among the promises of quantitative blood flow measurements are improved diagnostic accuracy, including the ability to overcome false-negative studies in the setting of balanced ischemia and improved risk stratification.[63,71–75] Quantitative MBF can be assessed globally and regionally.

As with all nuclear cardiology techniques, attention to quality control (e.g., assessment of time-activity curves) and use of validated methodology and software packages are crucial. It is also important to recognize the potential pitfalls when interpreting and reporting derived quantitative values, including the influence of various forms of stress, different radiotracers, characteristics of particular software packages, and even unique patient idiosyncrasies. In addition, as

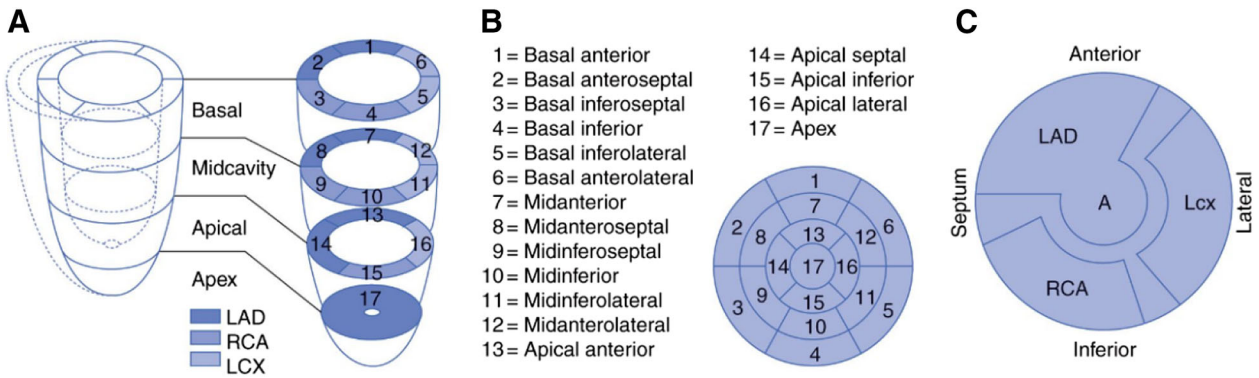

Figure 1. LV myocardial segmentation, standard nomenclature, and vascular territories. PET images are interpreted on the basis of the presence, location, extent, and severity of myocardial perfusion and metabolic defects using a standard 17-segment model and visual scoring. (A) The standard segmentation model divides the LV into three major short-axis slices: apical, mid-cavity, and basal. The apical short-axis slice is divided into four segments, whereas the mid-cavity and basal slices are divided into six segments. The apex is analyzed separately, usually from a vertical long-axis slice. (B) Data from the individual short-axis tomograms can be combined to create a polar map plot, representing a 2D compilation of all the 3D short-axis perfusion data. Standard nomenclature for the 17 segments is outlined. (C) The 2D compilation of perfusion data can then easily be assigned to specific vascular territories. (From Dilsizian V.; reprinted with permission).[55]

with most imaging parameters, MBF values should be supplements to be considered in conjunction with patient clinical characteristics and other image findings when used to diagnose and direct patient management.

At the present time, quantitative absolute MBF measurements with PET appear most helpful in:

1. Patients without known prior history of cardiac disease who present with symptoms suspicious for myocardial ischemia.
2. Patients with known CAD, in whom more specific physiological assessment is desired.
3. Identifying an increased suspicion for multivessel CAD.
4. Situations with a disparity between visual perfusion abnormalities and apparently normal coronary angiography, in order to assess possible microvascular dysfunction.
5. Heart transplant when there is a question of vasculopathy.

In contrast, there are particular patients for whom reporting hyperemic blood flow or flow reserve *may not add diagnostic value* or can be ambiguous or misleading, including:

1. Patients post-CABG who can have diffuse reduction on MBF despite patent grafts.
2. Patients with large transmural infarcts where resting flow may be severely reduced such that small increases in flow lead to normal or near-normal flow reserve.
3. Patients with advanced severe chronic renal dysfunction who likewise often have diffuse coronary disease.
4. Patients with severe LV dysfunction.

While hyperemic blood flow and flow reserve values may predict worse prognosis, it is already known that patients with prior CABG, prior MI, chronic renal failure, and/or severe LV dysfunction are at higher risk. Because many patients are referred for diagnosis and detection of ischemia to determine if revascularization therapy is an option, reporting flow and flow reserve under the above circumstances may mislead the referring physician or healthcare provider.

In addition, because of various potential patient (e.g., receptor peculiarities) and external reasons (e.g., unappreciated caffeine intake), a patient can be a non-responder to vasodilator stress, with a global MFR at or about 1. In such circumstances, the visual perfusion image findings may be invalid. Also, the stress portion of the test may need to be repeated ensuring no caffeine, or using another pharmacologic stress imaging agent.

While some variations in cut-off values have been reported for different tracers and different software, at the present time it is generally accepted that MFR values can be interpreted as follows (with small variation depending on software):

1. MFR >2.3 indicates a favorable prognosis (assuming that there is no lower regional value).
2. MFR <1.5 suggests significantly diminished flow reserve (in the absence of concomitant elevated resting blood flow), and is associated with elevated cardiac risk.

Quantitative assessment of MBF in absolute units (e.g., mL/min/gm tissue) has been well established in the literature with ^{13}N-ammonia and ^{15}O-water.[40–42,44,49–51,64] It requires the acquisition of images in dynamic mode. The use of list-mode acquisition enables flow quantification in conjunction with perfusion and gated LV and regional function. The added value in terms of diagnosis and prognosis is the subject of active investigation in several centers. Regions of interest are placed on the LV myocardium and the LV blood pool and are copied to all serially acquired images for generation of myocardial tissue and blood pool time-activity curves. The time-activity curves are corrected for activity spillover from the blood pool to the myocardium and for radioactive decay. They are then fitted with a validated tracer kinetic model, and estimates of MBF are obtained. Software programs are also available for generating parametric polar maps that display regional MBF in absolute units.

Quantification of MBF with ^{82}Rb has been more challenging because of its 75-second half-life resulting in noisy myocardial and blood pool time-activity curves.[76,77] Newer software packages have incorporated mathematical correction and improved quantitation of ^{82}Rb perfusion images. The kinetic behavior ^{82}Rb in tissue can be described by a one- or two-compartment model that can be fitted using the arterial input function (i.e., obtained from the blood pool concentration of the LV cavity or left atrium) and myocardial time-activity curves at each segment, or even (with sufficient statistics) at each pixel.[77–82] The parameters of the model, which include flow, can be estimated using non-linear regression or other techniques. The variability of flow estimates can be reduced by fixing certain parameters to physiologically realistic values.[83]

Gated PET images. The ability to acquire cardiac PET images in conjunction with ECG gating is an important development that has not always been available, particularly on 3D scanners. As with SPECT, accurate gating with PET requires regular R-R intervals.

Some systems, however, support ECG-gated imaging via list-mode acquisition that may allow accurate assessment of gated LV function in patients with irregular rhythms. In such a mode, the positions of all coincidence pairs are recorded along with timing information and input from an electrocardiogram. These data can be retrospectively processed to produce ECG-gated images, ungated images, and if necessary, dynamic images, which represent the activity distribution as a function of time. The flexibility of this mode of acquisition is particularly convenient for quantitative analysis.

ECG gating of the rest and peak-stress myocardial perfusion images can provide additional information regarding changes in LV function and volumes.[84] Unlike ECG gating of the post-stress SPECT images, PET acquisitions take place during peak pharmacologic vasodilation.[84,85] ECG gating of ^{18}F-FDG PET images can also provide additional information regarding regional and global LV function and volumes.

PET IMAGING OF GLUCOSE METABOLISM

^{18}F-FDG PET imaging is the only FDA-approved technique for the assessment of myocardial viability. Other disease entities in which metabolic imaging with ^{18}F-FDG PET can play an important role include the detection of inflammation, as in cardiac sarcoidosis, and for the detection of infections, as in cardiovascular devices and prosthetic valves. Depending on the disease process, measurements of glucose metabolism can reflect the rates of cellular glucose use from either cardiac myocytes or from pro-inflammatory cells that infiltrated either the myocardium or the vasculature. Consequently, PET with ^{18}F-FDG can be used to detect the increase in glucose metabolism in these cell types in a host of cardiovascular diseases.

Glucose Metabolism by the Cardiac Myocyte

For a given physiologic environment, the cardiac myocyte consumes the most efficient metabolic fuel as an adaptive response to meet its energy demands. Under fasting and aerobic conditions, long-chain fatty acids are the preferred fuel in the heart as they supply 65 to 70% of the energy for the working heart, and some 15 to 20% of the total energy supply comes from glucose.[86] In postprandial conditions, glucose becomes the preferred energy substrate. This rapid adaptation in substrate use is an essential component of maintaining normal cardiac function and is dependent on a host of variables such as substrate availability, hormonal status, cardiac workload, and other factors.[86–88] In contrast, chronic adaptations in cardiac myocyte substrate metabolism occur in response to sustained abnormal stimuli.[89–91] For example, the chronic reduction of MBF levels that occur with myocardial hibernation leads to an overdependence on glucose metabolism by the cardiac myocyte. In general, this metabolic change is adaptive and preserves cardiac myocyte health. In contrast, the sustained increases in plasma fatty acids that occur in diabetes mellitus result in a chronic increase in fatty acid metabolism and a reduction in glucose use. Although initially adaptive, this change in metabolism eventually becomes maladaptive and leads to cardiac dysfunction.

Glucose Metabolism by Pro-inflammatory Cells

Increased glucose metabolism is a hallmark of activation of immune cells involved in both innate (e.g., monocytes and macrophages) and adaptive (e.g., T and B cells) immunity.[92] The increase in glucose metabolism is triggered to meet the higher energy demands of immune cell activation and reflects the stimulation of key transcriptional and other signaling pathways. Thus, under pro-inflammatory conditions, such as sarcoidosis or device infection that are discussed below, the presence of immune cell infiltration and activation can be measured.

There are numerous radiotracers that can measure cellular glucose metabolism either directly, such as with ^{18}F-FDG and ^{11}C-glucose, or indirectly, such as ^{11}C-palmitate and the various ^{18}F fatty acid analogs. However, this document will only focus on measurements of glucose metabolism using ^{18}F-FDG because it is the only metabolic radiotracer that is FDA approved and is used routinely for clinical purposes. ^{18}F-FDG is used for the detection of viable myocardium where the increased cardiac myocyte glucose metabolism is a marker of cellular viability. More recently, ^{18}F-FDG is used to manage patients with potential cardiac sarcoidosis, medium-to-large vessel vasculitis, and cardiac device infection, where cellular inflammation is central to the pathogenesis of these disease processes. The performance of ^{18}F-FDG in these cardiac diseases is discussed below. It should be noted that ^{18}F-FDG is being used with increasing frequency to evaluate other cardiovascular diseases, such as right ventricular imaging due to pulmonary hypertension and vascular imaging in atherosclerosis. These applications, however, are primarily investigational in nature and will not be discussed further.

^{18}F-FDG metabolic imaging

Tracer properties. FDG competes with glucose for transport and for phosphorylation by hexokinase.

Different from glucose, the phosphorylated radiotracer, ^{18}F-FDG-6-phosphate does not proceed into glycogen synthesis or aerobic glycolysis with only minimal dephosphorylation and return of radiotracer to blood; it is thus metabolically trapped in tissue. Consequently, its uptake is reflective of overall glucose uptake. CMS has approved reimbursement of ^{18}F-FDG for the evaluation of myocardial viability. ^{18}F is produced in a cyclotron through the (p, n) reaction, consisting of bombardment of ^{18}O-enriched water,[93] and decays by the emission of a positron with a half-life of 110 minutes. The low kinetic energy of the positron, 511 keV, allows the highest spatial resolution among all PET radionuclides. The 110-minute physical half-life of ^{18}F-FDG allows sufficient time for synthesis and purification, with its commercial distribution in a radius of several hours from the production.

Tracer dosimetry. The effective dose for a 10-mCi dose of ^{18}F-FDG administered intravenously is 7 mSv. The critical organ is the urinary bladder wall which receives an effective dose of 48 mSv.[94] Frequent voiding 1 to 3 hours post-administration is recommended in order to reduce radiation exposure.

Detection of viable myocardium

Study protocol. Acute and chronic metabolic adaptation to a temporary or sustained reduction in coronary blood flow is designed to protect the structural and functional integrity of the myocardium. Reversible metabolic changes, as an adaptive measure to sustain myocardial viability, will occur in the setting of diminished, but not absent, regional MBF. When MBF is absent, irreversible metabolic changes will occur followed by myocardial infarction and cell death. Consequently, demonstration of preserved glucose metabolism by ^{18}F-FDG is a marker of myocardial viability. In general, the lack of glucose metabolism is indicative of non-viable myocardium. Accurate detection of viable myocardium is achieved by referencing the level of myocardial glucose metabolism to the level of MBF.

Typically, the measurements of MBF are performed with either ^{82}Rb or ^{13}N-ammonia using procedures described in the PET myocardial perfusion section. If these radiotracers are not available, MBF can be separately determined using technetium-99m-labeled myocardial perfusion SPECT radiotracers. Measurements of flow should be obtained in the same imaging session as measurements of myocardial glucose metabolism, regardless of the blood flow radiotracer that is used. If blood flow and metabolism data are acquired within a few weeks or months apart, it is important to verify that the patient has been stable during that time interval and there has been no change in symptoms or medications. Combining the information from the glucose metabolism and blood flow studies generate metabolism-flow patterns indicative of viable and non-viable myocardium.

Patient preparation. Because of the marked flexibility in substrate use by the myocardium, standardization of the substrate environment is of critical importance when performing cardiac ^{18}F-FDG PET imaging. The goals and protocols for standardization of the substrate environment differ depending upon whether the clinical indication for the study is to detect myocardial viability or inflammation. For the evaluation of myocardial viability with ^{18}F-FDG, the substrate and hormonal levels in the blood need to favor metabolism of glucose over fatty acids by the myocardium.[56,87,95,96] This maximizes the ^{18}F-FDG uptake in the myocardium, resulting in superior image quality, and reduces the regional variations in ^{18}F-FDG uptake that can occur when imaging under fasting conditions.[57] Protocols to standardize the substrate environment for viability imaging are shown in Tables 10 and 11.

Standardization is usually accomplished by loading the patient with glucose after a fasting period of at least 6 hours to induce an endogenous insulin response. The temporary increase in plasma glucose levels stimulates pancreatic insulin production, which in turn reduces plasma fatty acid levels through its lipogenetic effects of adipocytes and also normalizes plasma glucose levels.

The most common method of glucose loading is with an oral load of 25 to 50 grams, but IV loading is also used. The IV route avoids potential problems due to variable gastrointestinal absorption times or inability to tolerate oral dosage. Because of its simplicity, most laboratories utilize the oral glucose-loading approach, with supplemental insulin administered as needed. The physician should take into account whether or not the patient is taking medications that may either antagonize or potentiate the effects of insulin.

Diabetic patients. Diabetic patients pose a unique challenge, either because they have limited ability to produce endogenous insulin or because their cells are less able to respond to insulin stimulation. For this reason, the simple fasting/oral glucose-loading paradigm is often not effective in diabetic patients. Use of insulin along with close monitoring of blood glucose (Table 11) yields satisfactory results. Improved ^{18}F-FDG images can also be seen when image acquisition is delayed 2 to 3 hours after injection of the ^{18}F-FDG dose. Of course, the latter comes at the expense of increased decay of the radiopharmaceutical. An alternative technique is the euglycemic-hyperinsulinemic clamp, which is a rigorous and time-consuming procedure.[96] However, it allows close titration of the metabolic substrates and insulin levels, which results

Table 10. Patient preparation for ^{18}F-FDG PET cardiac viability assessment

Procedure	Steps for standardization	Technique
Fasting period	***Step 1*: Fast patient** 6-12 hours <6 hours ***Step 2:* Check blood glucose (BG) and the glucose load** (choose one of the following 3 options)	 Preferred Suboptimal
Oral glucose load	*Option 1*: Oral glucose loading **IF:** fasting BG <~250 mg/dL (13.9 mmol/L) **THEN:** 1) oral glucose load: typically 25-100 g orally, (see **Table 11**) 2) monitor BG (see Table 11) **IF**: fasting BG > ~250 mg/dL (13.9 mmol/L) **THEN:** see **Table 11**	Standard Standard
IV protocol	*Option 2:* Dextrose IV infusion See details, sample protocol, Appendix	Optional
Acipimox	*Option 3:* Acipimox Acipimox, 250 mg orally not available in the US ***Step 3:* Administer^{18} F-FDG**	
^{18}F-FDG injection	*Time:* Dependent on which option was selected Standard IV administration of ^{18}F-FDG, see **Table 12, item 1**	Standard
Begin PET imaging	0-90 minutes post ^{18}F-FDG injection, see **Table 12**	

Table 11. Guidelines for BG maintenance (after glucose administration) for optimal ^{18}F-FDG cardiac uptake, BG of approximately 100-140 mg/dL (5.55-7.77 mmol/L) at time of injection of ^{18}F-FDG

BG at 45-60 min after administration	Restorative measure	Technique
130-140 mg/dL (7.22-7.78 mmol/L)	1 U regular insulin IV	Standard
140-160 mg/dL (7.78-8.89 mmol/L)	2 U regular insulin IV	
160-180 mg/dL (8.89-10 mmol/L)	3 U regular insulin IV	
180-200 mg/dL (10-11.11 mmol/L)	5 U regular insulin IV	
> 200 mg/dL (>11.11 mmol/L)	Notify physician	
BG = blood glucose; FDG = fluorodeoxyglucose; IV = intravenous; mg = milligram; mmol = millimoles; L = liter; dL = deciliter; U = unit		

in excellent image quality in most patients and allows absolute quantification of myocardial glucose utilization. Shorter IV glucose/insulin-loading procedures of 30 minutes have also been used with some success.[58] (see ''Protocol'' section, Appendix).

Acquisition parameters. Acquisition parameters for ^{18}F-FDG PET cardiac imaging are itemized in Table 12. If ^{18}F-FDG PET metabolic images are compared to perfusion images acquired by SPECT, the interpreter should be mindful that there will be differences in soft tissue attenuation, image resolution, and registration problems of images acquired on different instruments. It should be noted that if a ^{201}Tl- or a ^{99m}Tc-labeled perfusion tracer is used to assess myocardial perfusion, there is no need to delay the ^{18}F-FDG PET images. ^{201}Tl and ^{99m}Tc will not interfere with the higher energy ^{18}F photons. However, with 3D PET imaging, the ^{99m}Tc activity can increase dead time and thus decrease the true counts from the ^{18}F-FDG. If ^{18}F-FDG PET images are acquired first, then it is necessary to wait at least 5 half-lives, depending on the dose of ^{18}F administered, before a low-energy (e.g., ^{201}Tl or ^{99m}Tc) SPECT study is performed. This is because the 511-keV photons from the PET tracers easily penetrate the collimators that are commonly used for ^{201}Tl or ^{99m}Tc imaging. Iterative reconstruction (ordered subset expectation maximization, OSEM, 21 subsets, 2 iterations) is the recommended method of image reconstruction.

Table 12. ^{18}F-FDG PET cardiac imaging acquisition guidelines for PET/CT and dedicated PET

Feature	Technique	Requirement
Tracer dose (2D or 3D)	5-15 mCi (185-555 MBq)	Standard
Injection rate (Static)	Not critical, bolus to 2 min	Standard
Injection rate (Dynamic)	Bolus for glucose quantification	Optional
Image delay after injection	45-60 min after injection (keep constant for repeat studies)	Standard
Patient positioning PET PET/CT	 Use an ^{18}F-FDG scout scan Use transmission scan CT scout scan	 Optional Standard Standard
Imaging mode	2D or 3D Static or list mode Dynamic	Standard Standard Optional
Image duration	10-30 min (depending on count rate and dose)	
Attenuation correction	Measure attenuation correction: before or immediately after scan	Standard
Reconstruction method	Iterative expectation maximization (e.g. OSEM) or FBP	Standard
Reconstruction filter	Sufficient to achieve desired resolution/smoothing, matched between consecutive studies	Standard
Reconstructed pixel size	2-3 mm 4-5 mm	Preferred Acceptable
Note: If metabolism imaging is combined with PET perfusion imaging, the same parameters for patient positioning, attenuation correction, and image reconstruction should be applied.		

Dose. Typically, 5 to 15 mCi of ^{18}F-FDG is injected in a peripheral vein. Injection speed is not critical (i.e., bolus to 2 minutes). To reduce patient dose to the bladder, patients should be encouraged to void frequently for 3 to 4 hours after the study.

Scan start time and duration. It is suggested to wait for a minimum of 45 minutes before starting the static ^{18}F-FDG scan acquisition. Myocardial uptake of ^{18}F-FDG may continue to increase, and blood pool activity to decrease, even after 45 minutes. While waiting for 90 minutes after the injection of ^{18}F-FDG may give better blood pool clearance and myocardial uptake, especially in diabetics or subjects with high blood glucose levels, this comes at the expense of reduced count rate. If target-to-background ratio is poor at 45 to 60 minutes, injecting an additional 1 to 3 units of insulin (depending on the blood glucose level) and then waiting for an additional 45 to 60 minutes may improve the image quality substantially. Scan duration is typically 10 to 30 minutes. If acquired in 3D mode, compared with 2D mode with the same machine, a smaller dose is typically required to achieve the same total count rate, but the imaging time may or may not be reduced as a result of count rate limitations and increased scatter. With some PET cameras, beyond a certain dose, the 3D mode will actually produce poorer quality images for the same dose and imaging time than 2D mode. For this reason, it is critical to have fully characterized the performance of the PET system.

Assessment of myocardial viability. Detection of viable myocardium plays a central role in the management of patients with LV dysfunction due to CAD.[97] It is based on the recognition that resting LV dysfunction may be reversible, attributable to myocardial hibernation/stunning, and not necessarily due to myocardial scar. As a consequence, its presence signifies a different prognosis and mandates a different treatment paradigm compared with the presence of predominantly non-viable or irreversible damaged tissue. Indeed, the importance of differentiating viable from non-viable tissue is highlighted by the plethora of techniques currently available to perform this task. Myocardial metabolism imaging with PET and ^{18}F-FDG uses the preservation of myocardial glucose metabolism, particularly in the presence of resting hypoperfusion as a scintigraphic marker of viable myocardium. It is accomplished with ^{18}F-FDG as a tracer of exogenous glucose utilization. The regional myocardial concentrations of this tracer are compared with the regional distribution of myocardial perfusion. Regional increases in ^{18}F-FDG

uptake relative to regional MBF (i.e., perfusion-metabolism mismatch) signify myocardial viability. In contrast, a regional reduction in ^{18}F-FDG uptake in proportion to regional reductions in myocardial perfusion (i.e., perfusion-metabolism match) signifies myocardial scar or non-viable tissue. Areas with maintained perfusion, but diminished ^{18}F-FDG uptake, also likely reflect regions of jeopardized but viable myocardium as the perfusion tracers reflect active metabolic trapping.

Comparison of myocardial metabolism to perfusion. The comparison of perfusion and metabolism images obtained with PET is relatively straightforward because both image sets are attenuation corrected. Thus, a relative increase in myocardial metabolism in regions of reduced perfusion by one grade or more reflects the presence of perfusion-metabolism mismatch, hence myocardial viability. In contrast, a relative decrease in myocardial metabolism that is in proportion to reductions in regional perfusion reflects the presence of perfusion-metabolism match, hence myocardial scar or non-viable tissue. Areas with maintained perfusion, but diminished ^{18}F-FDG uptake (termed reverse mismatch), also likely reflect regions of jeopardized but viable myocardium since the perfusion tracers reflect active metabolic trapping (Na-K ATPase system for ^{82}Rb and ^{13}N-glutamine mediated by ATP and glutamine synthetase for ^{13}N-ammonia).[43]

Special considerations for combining SPECT perfusion with PET metabolism images. In current clinical practice, ^{18}F-FDG PET images are often read in combination with SPECT myocardial perfusion images. The interpreting physician should be careful when comparing the non-attenuation-corrected SPECT images with attenuation-corrected ^{18}F-FDG PET images. Myocardial regions showing an excessive reduction in tracer concentration as a result of attenuation artifacts, such as the inferior wall in men or the anterior wall in females, may be interpreted as perfusion-metabolism mismatches, resulting in falsely positive perfusion-metabolism mismatches. Two approaches have proved useful for overcoming this limitation:

1. Because assessment of viability is relevant only in myocardium with regional contractile dysfunction, gated SPECT or PET images offer means for determining whether apparent perfusion defects are associated with abnormal regional wall motion.
2. Quantitative analysis with polar map displays that are compared with tracer- and gender-specific databases (for SPECT images) may be a useful aid to the visual interpretation. SPECT perfusion images with attenuation correction are helpful; however, neither approach is infallible.[98,99]

For myocardial ^{18}F-FDG images acquired with ultra-high-energy collimators or with SPECT-like coincidence detection systems, additional problems may be encountered, especially when the images are not corrected for photon attenuation.[100–103] Attenuation of the high-energy 511-keV photons is less than that for the 140-keV photons of ^{99m}Tc or the 60- to 80-keV photons of ^{201}Tl, so that attenuation artifacts are less prominent for ^{18}F-FDG images and may result in an apparent mismatch. Furthermore, the lower spatial resolution of SPECT imaging systems for ^{18}F-FDG imaging, especially when using high-energy photon collimation and then comparing with ^{99m}Tc or ^{201}Tl images, causes apparent mismatches for small defects, at the base of the LV, or at the edges or borders of large perfusion defects. Such artifacts resulting from the use of different photon energies can be avoided using dedicated PET systems for both perfusion and metabolism imaging. Again, use of ECG-gated imaging to demonstrate normal wall motion, quantitative analysis through polar map displays with comparison to radiotracer- and gender-specific databases of normal may aid in the visual interpretation.

Absolute myocardial glucose utilization. Quantitative estimates of myocardial glucose utilization in absolute units of micromoles of glucose per minute per gram of myocardium have not been found to aid in the assessment or characterization of myocardial viability due to the variability in substrate utilization by the myocardium, even when ^{18}F-FDG images are acquired during a hyperinsulinemic-euglycemic clamp.[95,96,104]

Methods for deriving quantitative estimates of myocardial metabolism require acquisition of serial images for 60 minutes that begin with tracer injection.[93,105] ROIs are placed on the myocardium and the LV blood pool and are copied to all serially acquired images in order to generate myocardial tissue and blood pool time-activity curves. The time-activity curves are corrected for spillover activity from the blood pool into the myocardium and for radioactive decay. The time-activity curves are then fitted with a validated tracer kinetic model, and estimates of regional myocardial glucose utilization are obtained in micromoles of glucose per minute per gram of myocardium. Measurements of glucose metabolic rates further require determination of glucose concentrations in arterial or arterialized venous blood. Similar to myocardial perfusion, parametric images and polar maps are also available for display of rates of regional myocardial glucose utilization. Regional metabolic rates on such parametric images are coded by a color scale and can be determined non-invasively for any myocardial region through ROIs assigned to the polar map.[106]

Integration of perfusion and metabolism results. The combined evaluation of regional myocardial perfusion and ^{18}F-FDG metabolism images allows identification of specific flow-metabolism patterns that are useful to differentiate viable from non-viable myocardium.[107–112] It is useful to start with a functional assessment, ideally from gated PET or SPECT imaging, as dysfunctional segments are those suitable for evaluation of myocardial viability. If stress perfusion images as well as resting perfusion images are available, jeopardized myocardium can be distinguished from normal myocardium, and myocardium perfused normally at rest, but dysfunctional as a result of repetitive stunning, can be distinguished from myopathic or remodeled myocardium.

Differences in blood pool concentration of tracers can impact the apparent match or mismatch of perfusion ^{18}F-FDG images. The separate adjustment of threshold and contrast settings can help compensate for these discrepancies.

Four distinct resting perfusion-metabolism patterns may be observed in dysfunctional myocardium. Patterns 1–2 are all indicative of viable myocardium, whereas pattern 3 represents non-viable tissue (Table 13).

If stress and rest perfusion imaging information is available, it is useful to add an estimate of the extent of stress-inducible ischemia in regions of normal resting perfusion and ^{18}F-FDG uptake, in regions with matched resting perfusion ^{18}F-FDG defects, or in regions with resting perfusion ^{18}F-FDG metabolic mismatch. The simultaneous display of stress and rest perfusion and ^{18}F-FDG metabolic images is most helpful but not available on all display workstations. In circumstances where only resting perfusion imaging is performed alongside ^{18}F-FDG metabolic imaging, besides reporting on the extent of scar and extent of hibernating myocardium, it is useful to indicate that in the absence of corresponding stress myocardial perfusion images, one cannot rule out stress-induced myocardial ischemia.

In circumstances where only stress perfusion imaging is available in combination with ^{18}F-FDG metabolic imaging, the following patterns can be found in segments with contractile dysfunction:

1. Stress perfusion defect with preserved ^{18}F-FDG uptake indicates ischemic but viable myocardium. Revascularization is generally appropriate as myocardial ischemia is a very strong predictor for recovery of perfusion and function after a successful revascularization. With stress perfusion and ^{18}F-FDG metabolic paired images, it is not possible to differentiate between myocardial ischemia, stunning, and hibernation.
2. Stress perfusion defects associated with proportionately decreased or lack of ^{18}F-FDG uptake indicates scarred or non-viable myocardium, and revascularization is not recommended.

Qualitative or semiquantitative approaches can be applied to the interpretation of perfusion-metabolism patterns. When comparing ^{18}F-FDG metabolism with perfusion images, it is important to first identify the normal reference region (the region with the highest tracer uptake), preferably on the stress myocardial perfusion images. The extent of mismatch or match defect may be small (5 to 10% of the LV), moderate (10 to 20% of the LV), or large (>20% of the LV). The severity of a match defect can be expressed as mild, moderate, or severe in order to differentiate between non-transmural and transmural myocardial infarction.

Interpretation of ^{18}F-FDG images when perfusion images have not been obtained. Interpretation of ^{18}F-FDG images without perfusion images and/or angiographic information and/or without information on regional wall motion is discouraged. The presence of relatively well-preserved ^{18}F-FDG uptake in dysfunctional myocardium does not differentiate ischemic from non-ischemic cardiomyopathy. The

Table 13. Interpretation of myocardial perfusion and glucose loaded ^{18}F-FDG patterns

Myocardial blood flow	^{18}F-FDG uptake	Interpretation
Normal blood flow	Normal ^{18}F-FDG uptake	Normal
Reduced blood flow	Preserved or enhanced ^{18}F-FDG uptake	Perfusion-metabolism mismatch
Normal or near-normal blood flow	Reduced ^{18}F-FDG uptake	Reversed perfusion-metabolism mismatch May occur in the septum of patients with LBBB[114]
Proportionally reduced blood flow	Proportionally reduced ^{18}F-FDG uptake	Perfusion-metabolism match
The first 3 patterns represent viable myocardium. Only the last pattern, where both perfusion and metabolism defects are matched, represents nonviable (scarred) tissue		

degree of ^{18}F-FDG accumulation over and above regional perfusion helps assess the relative amount of scar and metabolically viable myocardium. The latter information may significantly influence the power of the test for predicting functional recovery. Therefore, it is recommended that ^{18}F-FDG metabolic images be analyzed in conjunction with perfusion images, obtained either with SPECT or, preferably, with PET.

DETECTION OF INFLAMMATION AND INFECTION

^{18}F-FDG imaging is becoming an accepted tool for diagnosing active cardiac inflammation.[114,115] While the technique is potentially useful in a variety of inflammatory conditions, such as giant cell myocarditis[116] and viral myocarditis,[117] currently the predominant use is for identification of active cardiac sarcoidosis. Another emerging application is for identification of cardiovascular infections, particularly prosthesis and device infection.

Assessment of Cardiac Sarcoidosis

Sarcoidosis with cardiac involvement indicates a high risk of mortality and morbidity, accounting for 13% to 25% of fatal cases[118,119] with a reported five-year mortality ranging from 25% to 66%.[119,120] Signs and symptoms can be non-specific with autopsies showing more prevalent cardiac involvement than is appreciated clinically.[121] While a clinical diagnosis of cardiac sarcoidosis had customarily been established based on the Japanese Ministry of Health and Welfare Diagnostic Guidelines (JMHW)[122] as revised by the Japan Society of Sarcoidosis and other Granulomatous Disorders in 2006,[123] this standard relies on biopsy-proven cardiac involvement or histologically proven extra-cardiac disease with indirect findings of cardiac inflammation.[124] Unfortunately, cardiac biopsy has limited sensitivity. Indirect evidence consisted of cardiac ^{67}Ga (gallium citrate) uptake, a perfusion defect consistent with myocardial scarring, cardiac wall motion abnormalities, conduction abnormalities on ECG, and more recently abnormalities on cardiac MR.[125] Most recently, the value of cardiac ^{18}F-FDG PET imaging for assessment of active cardiac sarcoidosis has been demonstrated and in many places is becoming an established technique.[126–128] The Heart Rhythm Society has established new criteria for clinical diagnosis of cardiac sarcoidosis that includes PET imaging.[129]

The underlying pathophysiologic principle involves an upregulation of glucose metabolism at sites of macrophage-mediated inflammation. Diagnostic accuracy has been shown to be high, with a reported sensitivity of 89% and a specificity of 78%[125] from meta-analysis of 7 studies.[128] ^{18}F-FDG PET may be positive earlier than MR reflecting inflammatory activity of the disease.[130] In addition, strong risk-stratification power has been demonstrated for ^{18}F-FDG PET that is beyond that provided by the JMHW criteria.[131]

Study protocol. When ^{18}F-FDG PET is used for the detection of cardiac sarcoidosis, a rest perfusion imaging study is also required for both co-localization with the myocardium and to determine whether there are inflammatory cells present (termed mismatched defect) or absent (termed matched defect) in hypoperfused regions. For imaging of a cardiovascular device or prosthetic infections, or medium-to-large vessel vasculitis, however, a myocardial perfusion study is not required. Other than this difference in the requirement for a myocardial perfusion scan, the acquisition, reconstruction, image review, and reporting of the ^{18}F-FDG PET scan for infection/vasculitis are the same as for cardiac sarcoidosis.

For cardiac sarcoidosis, it is important to exclude significant obstructive CAD and prior myocardial infarction. CAD is excluded, prior to ^{18}F-FDG PET, preferably by a coronary angiogram (invasive or CT) or rest and stress MPI. The rest MPI study can be performed with either PET or SPECT methods. Rest MPI can be performed on the same day (typically) or on a different day (as needed) from the ^{18}F-FDG study. If SPECT MPI is used, attenuation-corrected images are recommended. MPI is required at baseline and at follow-up scans.

Patient preparation. A key aspect of cardiac sarcoidosis imaging is proper dietary preparation that suppresses physiological cardiomyocyte uptake of ^{18}F-FDG, such that tracer uptake is limited to active inflammatory cells in the myocardium (Table 14). The primary dietary preparation consisting of avoidance of carbohydrate-containing foods should begin about 24 hours prior to the test, with an intake of high-fat and high-protein foods for at least two meals 24 hours prior, and then an overnight fast.[132–136] Interpreting physicians should also be aware of potential confounding factors such as administration of glucose-containing IV medications and preparations to hospitalized patients, and less common activities, such as peritoneal dialysis. Suppression of myocyte glucose uptake can be assisted by giving IV unfractionated heparin (10 IU/kg 30 minutes prior + 5 IU/kg 15 minutes prior or 50 IU/kg 15 minutes prior to radiotracer administration)[137], which results in elevated[138] plasma levels of free fatty acids and increasing cardiac utilization of free fatty acids instead of glucose, without increasing partial thromboplastin time. Lower doses of IV heparin (15 IU/kg) appear to be effective in suppressing physiological uptake of ^{18}F-FDG without significant prolongation of partial thromboplastin time.

Although not systematically validated, a combination of one or more of the above methods appears to be

Table 14. Methods to suppress glucose utilization by normal myocardium

Methods	Technique	Comments
Prolonged fast	Fast of 12-18 hours	Preferred for patients on tube feeds or patients scheduled for procedures requiring NPO
High fat/low carbohydrate diet	Two meals 24 hours prior to the study, followed by an overnight fast	High fat, protein permitted, low-to-no carbohydrate diet
IV unfractionated heparin	15-50 units of regular IV heparin 15 min prior to IV ^{18}F-FDG administration *or* 500 IU of IV heparin 45 minutes and 15 minutes (total 1000 IU) prior to IV ^{18}F-FDG	Ensure patient has no contraindications to administration of IV heparin.* IV regular heparin drip is frequently prepared in D5W and should be discontinued whenever possible prior to the sarcoid protocol ^{18}F-FDG study.
Combined methods	High fat/low-carbohydrate diet for 2 meals, one day prior, followed by overnight fast, and IV regular heparin prior to administration of ^{18}F-FDG	

* including bleeding tendencies, allergy or history heparin-induced thrombocytopenia with thrombosis (HIT); IV = intravenous; NPO = Nil per os, nothing by mouth

better than any single method alone.[130] The success rates of these various methods to suppress the myocardial glucose utilization are not uniform, and may be difficult depending on the other factors, such as dietary compliance, medications, metabolic milieu, co-existing medical conditions, such as diabetes mellitus, etc.

^{18}F-FDG acquisition parameters. The acquisition parameters for ^{18}F-FDG cardiac scans are similar to those used for myocardial viability. Because a majority of these individuals also have cardiac devices, when hybrid PET/CT imaging is used, focal hot spots may be noted corresponding to the device leads. For this reason, both attenuation-corrected and non-attenuation-corrected images are reconstructed. Whenever feasible, a hybrid PET/CT scan may be preferable compared to a dedicated PET scan to localize region of ^{18}F-FDG uptake.

Dose. Typically, about 8 to 10 mCi of ^{18}F-FDG is injected intravenously into a peripheral vein manually or using an automatic injection system. Use of an automatic injection system (1 mL/s) may significantly reduce occupational radiation exposure to the technologists.[139] The height and weight of the patient and the preinjection and the post-injection doses (subtracting residual activity) are logged into the acquisition computer. This information is critical for estimating standardized radiotracer uptake values. It is important to keep the dose, injection-to-scan time, method of radiotracer dose (with or without residual subtraction), and the acquisition parameters similar for any follow-up scans.

Scan start time and duration. ^{18}F-FDG imaging is started 90 minutes (minimum of 60 minutes) after injection of radiotracer to allow for accumulation of radiotracer in the inflamed tissue. The acquisition includes a partial whole-body scan to include the lungs and mediastinum (3 minutes per bed position for 3D imaging, and 4 minutes per bed position for 2D scans) followed by a dedicated cardiac scan (10 minutes per bed position for 3D, 20 to 30 minutes for 2D imaging). The whole-body scan is repeated at follow-up.

Image interpretation of cardiac inflammation: sarcoidosis. As with viability studies, an accompanying MPI study, preferably with a PET tracer, such as ^{82}Rb or ^{13}N-ammonia, is important and considered essential by most practitioners. If a SPECT tracer is used for perfusion imaging, attenuation correction should be performed. Perfusion and ^{18}F-FDG slices should be displayed side by side using a conventional cardiac display, i.e., standard short-axis, horizontal long-axis, and vertical long-axis views. A semiquantitative scoring system, such as that used for perfusion and

viability studies, can be employed. ^{18}F-FDG ''hot spots'' identify areas of abnormal cardiac inflammation, as opposed to ''cold spots,'' which identify abnormalities of perfusion or metabolic viability.

Several methods of image interpretation pattern classification have been described, but none of these are formally established or validated with histological findings. One method focuses on ^{18}F-FDG uptake, and classifies findings as no uptake, diffuse uptake, focal uptake, and focal-on-diffuse uptake. Another incorporates perfusion and ^{18}F-FDG information, and classifies as normal perfusion and normal (i.e., absent) ^{18}F-FDG, either abnormal perfusion or abnormal ^{18}F-FDG, and both abnormal perfusion and abnormal ^{18}F-FDG.[140] Yet another group has classified in terms of perfusion and FDG patterns.[141] These classification schemes can help not only with initial diagnosis, but also to follow up disease progression and response to therapy.

Observation of ^{18}F-FDG limited to the cardiac blood pool suggests proper preparation and more confidently rules out active cardiac sarcoidosis. On the other hand, diffuse homogeneous cardiac uptake of ^{18}F-FDG, particularly in the absence of defects on accompanying perfusion imaging, may indicate inadequate suppression of cardiomyocyte ^{18}F-FDG uptake and may lead to a false-positive conclusion.

As with metabolic images, interpretation of images for the presence of active sarcoidosis inflammation must consider clinical data that might confound image findings. An important caveat to consider is some of the aforementioned patterns, such as regions with perfusion abnormalities that have increased ^{18}F-FDG uptake, could potentially indicate myocardial hibernation in the setting of ischemic heart disease. Thus, a diagnosis of active cardiac sarcoidosis may be difficult, if not impossible, in patients who also have coronary disease with ongoing ischemia.

Another issue is how to interpret diffuse ^{18}F-FDG uptake, which may be a consequence of poor dietary preparation. A focal-on-diffuse pattern suggests disease, having been reported in about 31% of patients with sarcoidosis.[142] On the other hand, focal ^{18}F-FDG uptake in the lateral wall and a diffuse basal pattern have been observed in healthy humans.[143]

It is also important to recognize that in this type of study, cardiac ^{18}F-FDG uptake indicates inflammation, which, while consistent with active sarcoidosis, can also be caused by a variety of inflammatory disease processes other than sarcoidosis. This concept needs to be indicated in the report. Findings may be ''consistent with'' but are never diagnostic of cardiac sarcoidosis, as tissue is required for diagnostic certainty.

Image interpretation may be enhanced by quantifying ^{18}F-FDG uptake using an SUV within each segment of the heart. SUVs represent the decay-corrected uptake in the tissue divided by the injected dose of tracer adjusted for body weight.[144] A maximal SUV greater than mean values plus two standard deviations from control patients have been suggested as an abnormal threshold,[141] with one report describing a sensitivity of 85% and a specificity of 90% in reference to JMHW criteria.[132] SUV values have been shown potentially useful in following patient response to therapy, having been shown to be associated with response to immunosuppressive therapy[145] and improvement in LV function.[146] A coefficient of variation of regional myocardial SUV, which represents ^{18}F-FDG uptake heterogeneity, may also help increase diagnostic accuracy, with a value >0.18 in one study demonstrating a sensitivity of 100% and a specificity of 97%, with a decrease in coefficient of variance seen after corticosteroid therapy.[124]

A whole-body ^{18}F-FDG PET, as well as CT transmission image (for hybrid scanning), should also be reviewed and reported for evidence of extra-cardiac sarcoid disease activity. Non-cardiac areas of ^{18}F-FDG uptake are potentially accessible biopsy sites for a definitive diagnosis of sarcoidosis. Whole-body scans can also provide a ratio of cardiac ^{18}F-FDG uptake to other regions, such as liver, cerebellum, and blood pool that may assist in diagnosing cardiac sarcoidosis and following response to therapy.

Assessment of Cardiovascular Device Infections

Use of cardiac implantable electronic devices (CIEDs), including pacemakers, cardiac resynchronization therapy devices, and implantable cardiac defibrillators (ICDs), as well as left ventricular assist devices (LVADs), and prostheses, such as valves and annular ring implants, have become key aspects of cardiac care. Despite well-established benefits in appropriate situations, there is a risk of device infection that has been increasing, with a reported CIED infection rate of 1.9/1000 device-years and associated blood stream infection or device-related endocarditis at 1.14/1000 device-years.[147,148] There are both intravascular and extravascular components, and infection can involve the generator, device leads, or native cardiac structures.[148]

Device infection carries a high risk of death if not identified and treated appropriately.[149] While transesophageal echocardiography is customarily the initial diagnostic approach, imaging of localized inflammation using radionuclide techniques shows potential for improving diagnostic accuracy.[150–156] One approach is to use white blood cells labeled with indium-111 or ^{99m}Tc. Factors that may limit the sensitivity of a radio-labeled white blood cell scan include the viability of the white blood cells after in vitro labeling process and the migration rate of the cells to the infection site. The latter becomes a

particular concern in patients who are on antibiotic treatment, in whom cell chemotaxis is decreased. In addition, this technique can be cumbersome and costly, and images are often count-poor with low spatial resolution. Different from radio-labeled white blood cell scintigraphy, ^{18}F-FDG PET/CT imaging is based on in vivo ^{18}F-FDG labeling of the pre-existing inflammatory cells at the infection site. With the stimulation of cytokines, these cells (macrophages, neutrophils, and lymphocytes) overexpress the glucose transporter-1 and accumulate ^{18}F-FDG with high concentration.[150] Thus, ^{18}F-FDG PET/CT for in vivo labeling of metabolically active inflammatory cells at the infection site has the advantage of superior tomographic images with higher spatial and contrast resolution, being less labor intensive, and giving less radiation exposure. ^{18}F-FDG PET/CT can accurately diagnose infection and, for devices such as an ICD or pacemaker, may help distinguish deep pocket from superficial infections.[150–152] Lead infection can sometimes also be identified, but is less diagnostically reliable.

Use of ^{18}F-FDG PET/CT for diagnosing cardiovascular device infection is based mainly on studies with relatively small patient cohorts, and needs further development. Although there are no accepted interpretation standards at this time, for CIEDs the following are techniques and issues to consider:[152]

1. Proper dietary preparation, as described in the prior sarcoidosis section, is to avoid confusing myocardial uptake from radiotracer activity in devices or prostheses next to or within the heart. Patients should avoid carbohydrates in the meal for 24 hours before the test and then fast overnight.
2. Both CT attenuation-corrected and non-attenuation-corrected images should be reviewed to help recognize artifacts of increased tracer uptake related to the high-density metal in devices. Any ''positive'' ^{18}F-FDG uptake on attenuation-corrected images should be confirmed on non-attenuation-corrected images.
3. Sites of abnormal ^{18}F-FDG PET/CT uptake should be noted as well as sites of maximal uptake.
4. Site of abnormal uptake should be separated by areas: skin (superficial), subcutaneous tissue, region surrounding the generator, overlying leads, and intravascular/intracardiac.

A qualitative visual score can be used:

Tracer uptake	Score
No tracer uptake	0
Mild tracer uptake (≤ lung parenchyma score)	1
Moderate tracer uptake (more intense than lung parenchyma)	2
Intense tracer uptake	3

5. Fused PET/CT images can be used to provide anatomic location for tracer uptake sites in relation to device components, i.e., generator, leads. The anatomic overlay can help distinguish device from superficial skin infection.
6. Distribution and pattern of tracer uptake may be more important than intensity of uptake. Focal or heterogeneous uptake favors infection, while mild diffuse uptake along a device or lead may favor non-specific inflammatory changes.

Regarding PET/CT imaging for LVAD-associated infections, the literature is sparse, consisting of case reports.[152] Infection can be identified on and around the pump, and along drivelines and cannula; however, specific criteria for image interpretation have not been developed.

Diagnosis of prosthetic valve endocarditis is challenging. While customarily echocardiographic techniques and blood cultures are the major criteria for making the diagnosis, each of these has limitations. ^{18}F-FDG PET/CT can facilitate the diagnosis of prosthetic valve endocarditis increasing sensitivity from 70% to 97% in relation to the modified Duke criteria, without decreasing specificity.[107,153] The following are issues to consider when performing and interpreting ^{18}F-FDG PET/CT imaging for suspected prosthetic valve endocarditis:

- Inflammatory activity may cause false-positive ^{18}F-FDG PET/CT results, such as early after prosthetic implantation.
- Surgical adhesive used to seal an aortic root graft may produce inflammation resulting in false-positive tracer uptake.[154]
- Small vegetations may cause false-negative results.
- Physiologic myocardial uptake of ^{18}F-FDG PET/CT and cardiac motion can interfere with proper image interpretation.

Currently, ^{18}F-FDG PET/CT imaging is not considered an initial or confirmatory study for prosthetic valve endocarditis.[155] At this time, the technique appears most useful for patients with suspicion of endocarditis but with indeterminate or negative clinical, echocardiographic, or microbiological findings.

REPORTING OF MYOCARDIAL PERFUSION AND METABOLISM PET STUDIES

Patient Information

The report should start with the date of the study, patient's age, sex, height, and weight or body surface area, as well as the patient's medical identification number.

Indication for Study

Understanding the reason(s) why the study was requested helps in focusing the study interpretation on the clinical question asked by the referring clinician. In addition, a clear statement for the indication of the study has become an important component of billing for services rendered. For sarcoidosis and infection studies, list prior clinical findings or correlative imaging results that led to consideration of the ^{18}F-FDG PET scan.

History and Key Clinical Findings

A brief description of the patient's clinical history and findings can contribute to a more appropriate and comprehensive interpretation of the rest (and stress) perfusion and of the metabolism images. This information may include past myocardial infarctions and their location, revascularization procedures, the patient's angina-related and congestive heart failure-related symptoms, presence of diabetes or hypertension, and other coronary risk factors. Information on regional and global LV function can similarly be important for the interpretation of regional perfusion and metabolism patterns.

A description of the ECG findings may serve as an aid in the study interpretation, such as the presence of Q-waves and their location or conduction abnormalities (e.g., LBBB) for exploring septal perfusion and/or metabolic abnormalities. A list of current cardiac medications should be included. For sarcoidosis and cardiovascular infection studies, identify if this is the initial study or follow-up study and list current immunosuppressive and infection therapy, respectively.

Type of Study

The imaging protocols should be stated concisely. This should include the type of camera utilized for imaging myocardial perfusion and/or metabolism, for example, PET or PET/CT system, or SPECT perfusion and ^{18}F-FDG PET metabolism. For stress myocardial perfusion PET studies, the type of stressor should be clearly indicated, such as treadmill, dipyridamole, adenosine, regadenoson (A_{2A} adenosine receptor agonist), or dobutamine. Radiopharmaceuticals and their radioactivity doses used for the perfusion and the metabolism PET imaging studies should be identified. The acquisition modes and image sequences should be described, such as static or dynamic image acquisition, for stress and rest perfusion imaging, perfusion and metabolism imaging on different days, and the use of gating.

The main body of the report following this introductory descriptive information should then be tailored to the specific clinical question asked by the referring clinician and the procedural approach chosen for answering this question.

Summary of Stress Data

If myocardial perfusion has been evaluated during stress, the type of the stressor, the stress agent, the dose, route of administration, and time of infusion should be specified. Side effects and symptoms experienced during stress should be reported. If pharmacologic stress was discontinued prematurely, the reasons should be provided.

Hemodynamic and ECG responses during the stress study, including changes in heart rate, blood pressure, development of arrhythmias, conduction abnormalities, and ST-T wave changes and their location, should be detailed. Symptoms such as chest pain, shortness of breath, and others during the administration of the stressor and in the recovery phase should be documented.

Summary of Clinical Laboratory Data and Dietary State

Information about the dietary state (e.g., fasting or postprandial) and about interventions for manipulating plasma glucose levels through, for example, oral or IV administration of glucose or use of the euglycemic-hyperinsulinemic clamp, should be given. If pharmacologic measures, such as nicotinic acid derivatives, have been used, this should be described. Furthermore, blood glucose levels, if obtained at baseline or after intervention, should be listed, as they are useful for the interpretation of the metabolic images. If there is an expected abnormal response to a glucose load, this should also be reported.

For sarcoidosis and cardiovascular infection studies, list the dietary preparation used to suppress glucose utilization by normal myocardium and the method used to interpret ^{18}F-FDG uptake (relative or SUV values).

Image Description and Interpretation: Perfusion

A statement regarding image quality is important. Reduced quality may affect the accuracy of the interpretation. If the cause of the reduced quality is known or suspected, then it should be stated accordingly. This information may prove useful when repeat images are obtained in the same patient.

The report should first describe the relative distribution of the perfusion tracer on the stress images and provide details on regions with decreased radiotracer uptake in terms of the location, extent, and severity of

defects that may be supplemented by a diagram. The authors should then describe whether regional myocardial defects seen on stress images become reversible or persist on the corresponding paired rest images. Other findings, such as LV cavity dilatation at rest, transient (stress-induced) LV cavity dilatation, lung uptake, concentric LV hypertrophy, asymmetric septal hypertrophy, pericardial photopenia, prominent RV cavity size and hypertrophy, and extra-cardiac abnormalities, should be included in the report. Regional and global LV function should be described from gated PET perfusion and/or metabolism images. The scintigraphic pattern on the stress/rest myocardial perfusion images should then be reported in clinical terms as:

1. Normal.
2. Ischemic.
3. Fixed defect. This should be considered scarred if there is a history of prior myocardial infarction or pathologic Q-waves on the ECG. However, in the absence of prior myocardial infarction or ECG Q-waves, particularly in patients with new-onset heart failure, hibernating but viable myocardium should be considered and assessed with additional myocardial viability study.
4. An admixture of scarred and ischemic but viable myocardium.
5. Non-ischemic cardiomyopathy.

Quantitative assessment of absolute regional MBF can be presented as an adjunct to the visual interpretation in the proper patient population.

Image Description and Interpretation: Metabolism for Myocardial Viability, Sarcoidosis, and Cardiovascular Infection

^{18}F-FDG myocardial viability study. The report should describe the relative distribution of myocardial perfusion at rest, and the location, extent, and severity of regional perfusion defects. The report should continue with a description of the ^{18}F-FDG uptake in the myocardium and indicate the tracer activity concentrations in normally perfused and in hypoperfused myocardium. The adequacy of achieving a glucose-loaded state, as evident from the radiotracer uptake in normally perfused myocardium and also from blood pool activity, should then be reported and be related to the presence of insulin resistance, including impaired glucose tolerance and type 2 diabetes. This should be related to the residual blood pool activity as additional evidence for inadequate clearance of ^{18}F-FDG from blood into tissue and provide the information for low tracer uptake in normally perfused myocardium. Segments with regional dysfunction that exhibit patterns of viable myocardium (i.e., preserved perfusion or decreased perfusion with relatively increased ^{18}F-FDG uptake) should be identified. Similar reporting should be performed for segments exhibiting a flow-metabolism matched pattern, that is, decreased regional ^{18}F-FDG uptake in proportion to decreased regional myocardial perfusion. The presence of viable and non-viable tissue should be reported as a continuum (e.g., predominantly viable or admixture of viable and non-viable tissues).

Findings on semiquantitative or quantitative image analysis, supplemented by a diagrammatic approach, may be added. Location and, in particular, extent of viable and non-viable tissues, expressed as a percentage of the LV, is important because it provides important prognostic information on future cardiac events and predictive information on potential outcomes in regional and global LV function, congestive heart failure-related symptoms, and long-term survival after revascularization. Finally, the description of the perfusion-metabolism findings may include a correlation to regional wall motion abnormalities and should indicate the potential for a post-revascularization improvement in the regional and global LV function. The potential for outcome benefit may also be reported.

^{18}F-FDG sarcoidosis/infection study. A statement regarding image quality and adequacy of suppression of glucose utilization by normal myocardium is important. Incomplete suppression of glucose utilization by normal myocardium may reduce the accuracy of the interpretation.

For sarcoidosis and infection ^{18}F-FDG studies wherein whole-body images are obtained, the whole-body ^{18}F-FDG findings should be reported. Sarcoidosis is a systemic disease and systemic disease activity may be important for management. Regions of abnormal ^{18}F-FDG uptake that may be accessible for biopsy should be reported. For infection studies, if distal septic embolization sites are identified, they should be reported.

Final interpretation. Results should be succinctly summarized and first addressed whether the study is normal or abnormal. On rare occasions where a definitive conclusion cannot be made, the interpreter should aid the referring clinician by suggesting other tests that may provide further insight into the clinical dilemma. The report should always take into consideration the clinical question that is being asked: is the study requested for CAD detection or myocardial viability assessment? Any potential confounding artifacts or other quality concerns that significantly impact the clinical interpretation of the PET study should be mentioned.

A statement on the extent and severity of perfusion defects, reversibility and mismatch in relation to ^{18}F-FDG metabolism, and their implication regarding ischemia,

scar, or hibernating myocardium should be made. It may be useful to conclude the report with a summary of the extent and location of myocardial ischemia in relation to vascular territories, as well as the presence and extent of perfusion-metabolism mismatch in patients with chronic ischemic LV dysfunction. LV cavity size, function, and regional wall motion should be reported at rest and during stress with special note of transient ischemic cavity dilatation, if present. A statement as to the implication of the findings should be made.

Comparison should be made to prior studies, and interim changes regarding the presence and extent of myocardial ischemia, scar, or hibernation should be highlighted. On the basis of the scintigraphic findings (e.g., extent of perfusion-metabolism mismatch), the likelihood of recovery of function after revascularization can be estimated. The potential for a post- revascularization improvement in contractile function is low for perfusion-metabolism matched defects, even if the regional reductions in perfusion and in ^{18}F-FDG uptake are only mild or moderate. Conversely, the potential for improvements in regional contractile dysfunction is high if perfusion is normal, if both perfusion and ^{18}F-FDG uptake are normal, or if ^{18}F-FDG uptake is significantly greater than regional perfusion (i.e., mismatch). Finally, the potential of a post-revascularization improvement in the LVEF by at least 5 or more EF units is high if the mismatch affects 20% or more of the LV myocardium,[108,156] although lesser amounts of mismatch (5 to 20% of the LV myocardium) may also have potential outcome benefit, with or without improvement in the LVEF.[157,158] The latter may be included in the report at the reporting physician's discretion.

For sarcoidosis and infection studies which are hot spot images, comparison to prior studies is based on SUV values or ratio of relative uptake in relation to another organ. Changes in response to therapy are indicated as changes in SUV. Comparison to prior studies, cardiac MR or echocardiography, when available may be helpful.

If additional diagnostic clarification seems to be needed, the physician may recommend an alternative modality. If a CT transmission scan was performed for attenuation correction, clinically relevant CT findings must be reported.

Disclosure

Dr. Rob S. Beanlands is a consultant to Lantheus Medical Imaging and Jubilant DRAXImage and receives grant support from Lantheus Medical Imaging, Jubilant DRAXImage, and GE Healthcare; Dr. Robert J. Gropler is a consultant to Biomedical Systems; Dr. Juhani Knuuti is a consultant to Lantheus Medical Imaging and serves on the speakers bureaus of GE Healthcare and Philips. All other contributors have nothing relevant to disclose.

APPENDIX: SAMPLE IV PROTOCOL

A sample protocol for IV glucose loading, based on one in use at Vanderbilt University Medical Center, Nashville, TN, and adapted from Martin et al[58] is presented.

1. IV glucose/insulin loading for non-diabetic patients with a blood glucose (BG) level <110mg/dL (<6.11 mmol/L) under fasting condition.
   a. Prepare dextrose/insulin solution: 15 U of regular insulin in 500 mL of 20% dextrose in a glass bottle. The initial 50 mL is discarded through the plastic IV tubing (no filter) to decrease adsorption of the insulin to the tubing.
   b. Prime the patient with 5 U of regular insulin and 50 mL of 20% dextrose (10g) IV bolus.
   c. Infuse dextrose/insulin solution at a rate of 3 mL kg^{-1} h^{-1} for 60 minutes (corresponding to an insulin infusion of 1.5 mU kg^{-1} min^{-1} and a glucose infusion of 10 mg kg^{-1} min^{-1}). Monitor BG every 10 minutes (goal BG, 100 to 200 mg/dL [5.56 to 11.11 mmol/L]).
   d. If BG at 20 min is 100-200 mg/dL (5.56 to 11.11 mmol/L), preferably <150 mg/dL (8.33 mmol/L), administer ^{18}F-FDG intravenously.
   e. If BG is >200 mg/dL (>11.11 mmol/L), administer small IV boluses of 4 to 8 U of regular insulin until BG decreased to <200 mg/dL (<11.11 mmol/L). Administer ^{18}F-FDG intravenously.
   f. Stop dextrose/insulin infusion at 60 minutes and start 20% dextrose at 2 to 3 mL kg^{-1} h^{-1}.
   g. During image acquisition, continue infusion of 20% dextrose at 2 to 3 mL kg^{-1} h^{-1}.
   h. At completion of the acquisition of the images, discontinue infusion, give a snack to the patient, and advise him or her regarding the risk of late hypoglycemia.
   i. ALERT:
      (i) If BG is >400 mg/dL (>22.22 mmol/L), call the supervising physician immediately.
      (ii) If BG is <55 mg/dL (<3.06 mmol/L) or if the patient develops symptoms of hypoglycemia with BG < 75 mg/dL (<4.17 mmol/L), discontinue dextrose/insulin infusion, administer one amp of 50% dextrose intravenously, and call the supervising physician.
2. IV glucose/insulin loading for diabetic patients or fasting BG is >110 mg/dL (>6.11 mmol/L):
   a. Prepare insulin solution: 100 U of regular insulin in 500 mL of normal saline solution in a glass bottle. The initial 50 mL is discarded through the

plastic IV tubing (no filter) to decrease adsorption of the insulin to the tubing.

b. Prime patient with regular insulin: If fasting BG is >140 mg/dL (>7.76 mmol/L), prime the patient with 10 U of regular insulin IV bolus. If fasting BG is <140 mg/dL (<7.76 mmol/L), prime the patient with 6 U of regular insulin IV bolus.

c. Infuse insulin solution at a rate of 1.2 mL kg^{-1} h^{-1} for 60 minutes (corresponding to an insulin infusion of 4 mU kg^{-1} min^{-1}) or for the entire study (to calculate the regional glucose utilization rate).

d. After 8-10 minutes or when BG is <140 mg/dL (<7.76 mmol/L), start 20% dextrose infusion at 1.8 mL kg^{-1} h^{-1} (corresponding to a dextrose infusion of 6 mg kg^{-1} min^{-1}).

e. Monitor BG every 5 to 10 minutes and adjust dextrose infusion rate to maintain BG at 80 to 140 mg/dL (4.44 to 7.76 mmol/L).

f. After 20 to 30 minutes of stable BG, administer ^{18}F-FDG.

g. Maintain the IV infusion of insulin plus 20% dextrose for 30 to 40 minutes after ^{18}F-FDG injection or until the end of the scan (to calculate rMGU [rate of glucose utilization]). Some centers confirm ^{18}F-FDG uptake particularly in patients with diabetes before discontinuing the clamp.

h. At completion of the acquisition of the images, discontinue infusion, give a snack to the patient, and advise him or her regarding the risk of late hypoglycemia.

3. For lean patients with type 1 juvenile-onset diabetes mellitus, apply the following protocol:

   a. If fasting BG is <140 mg/dL (<7.76 mmol/L), inject 4 U of regular insulin and infuse insulin solution at 0.3 mL kg^{-1} h^{-1} (1 mU kg^{-1} min^{-1}).

   b. After 8-10 minutes of infusion or when BG is <140 mg/dL (<7.76 mmol/L), start 20% dextrose at 2.4 mL kg^{-1} h^{-1} (8 mg kg^{-1} min^{-1}).

4. Some centers (Munich, Ottawa, and others) have also applied a front-loaded infusion.

   a. About 6 hours after a light breakfast and their usual dose of insulin or oral hypoglycemic, all diabetic patients have a catheter inserted in one arm for glucose and insulin infusion, as well as a catheter in the opposite arm for BG measurement.

   b. At time 0, the insulin infusion is started. Regular insulin is given at 4 times the final constant rate for 4 minutes, then at two times the final constant rate for 3 minutes, and at a constant rate for the remainder of the study.

   c. If the BG is >200 mg/dL (>11.11 mmol/L), an additional bolus of insulin is given. An exogenous 20% glucose infusion is started at an initial rate of 0.25 mg kg^{-1} min^{-1} and adjusted until stead state is achieved. The BG concentrations are measured every 5 minutes during the insulin clamp. The glucose infusion is adjusted according to the plasma glucose over the preceding 5 minutes.

References

1. Bacharach SL. Positron emission tomography. In: Dilsizian V, Pohost GM, editors. Cardiac CT, PET, and MR. 2nd ed. Hoboken: Wiley-Blackwell; 2010. p. 3-29.
2. Dilsizian V. 2014 SNMMI highlights lecture: Cardiovascular imaging. J Nucl Med 2014;55:9N–15N.
3. White JA, Rajchl M, Butler J, Thompson RT, Prato FS, Wisenberg G. Active cardiac sarcoidosis: First clinical experience of simultaneous positron emission tomography–magnetic resonance imaging for the diagnosis of cardiac disease. Circulation 2013;127:e639–41.
4. Dilsizian V, Bacharach SL, Beanlands SR, Bergmann SR, Delbeke D, Gropler RJ et al. ASNC Imaging Guidelines for Nuclear Cardiology Procedures: PET myocardial perfusion and metabolism clinical imaging. J Nucl Card 2009;16(4):651. American Society of Nuclear Cardiology website. http://www.asnc.org/files/PET%20MP%20&%20Glucose%20Metabolism%202009.pdf. Accessed December 15, 2015.
5. National Electrical Manufacturers Association. NEMA Standards Publication NU 2-2012. Performance measurements of positron emission tomographs. National Electrical Manufacturers Association website. http://www.nema.org/Standards/Pages/Performance-Measurements-of-Positron-Emission-Tomographs.aspx.
6. National Electrical Manufacturers Association. NEMA Standards Publication NU 2-1994. Performance measurements of positron emission tomographs. Washington, DC: National Electrical Manufacturers Association; 1994.
7. National Electrical Manufacturers Association. NEMA standards publication NU 2-2001. Performance measurements of positron emission tomographs. Washington, DC: National Electrical Manufacturers Association; 2001.
8. National Electrical Manufacturers Association. NEMA standards publication NU 2–2007. Performance measurements of positron emission tomographs. Rosslyn, VA: National Electrical Manufacturers Association; 2007.
9. American College of Radiology. ACR technical standard for medical nuclear physics performance monitoring of PET imaging equipment. Revised 2011 (Resolution 2). American College of Radiology website. http://www.acr.org/~/media/79b2f5688db3457fab228e311434abe8.pdf. Accessed November 20, 2015.
10. deKemp RA, Yoshinaga K, Beanlands RS. Will 3-dimensional PET-CT enable the routine quantification of myocardial blood flow? J Nucl Cardiol 2007;14:380–97.
11. Thomas L, Joel K. PET systems (Chapter 10). In: Wernick Miles N, Aarsvold John N, editors. Emission tomography. San Diego: Elsevier Academic Press; 2004. p. 179–94.
12. Lewellan T. Time-of-flight PET. Semin Nucl Med 1998;28:268–75.
13. Ter-Pogossian MM, Ficke DC, Yamamoto M, Hood JT. Super PETT I: a positron emission tomograph utilizing photon time-of-flight information. IEEE Trans Med Imaging 1982;1:179–87.

14. Yamamoto M, Ficke DC, Ter-Pogossian MM. Experimental assessment of the gain achieved by the utilization of time-of-flight information in a positron emission tomograph (Super PETT I). IEEE Trans Med Imaging 1982;1:187–92.
15. Suda M, Onoguchi M, Tomiyama T, Ishihara K, Takahashi N, Sakurai M, et al. The reproducibility of time-of-flight PET and conventional PET for the quantification of myocardial blood flow and coronary flow reserve with N-13 ammonia. J Nucl Cardiol 2015. doi:10.1007/s12350-015-0074-y.
16. Dorbala S, Di Carli MF, Delbeke D, Ishihara K, Takahashi N, Sakurai M, et al. SNMMI/ASNC/SCCT guideline for cardiac SPECT/CT and PET/CT 1.0. J Nucl Med 2013;54:1485–507.
17. Le Meunier L, Maass-Moreno R, Carrasquillo JA, Dieckmann W, Bacharach SL. PET/CT imaging: Effect of respiratory motion on apparent myocardial uptake. J Nucl Cardiol 2006;13:821–30.
18. American College of Radiology. ACR–AAPM technical standard for diagnostic medical physics performance monitoring of computed tomography (CT) equipment. Revised 2012 (Resolution 34). American College of Radiology website. http://www.acr.org/~/media/1C44704824F84B78ACA900215CCB8420.pdf. Accessed February 1, 2016.
19. Gould KL, Pan T, Loghin C, Johnson NP, Guha A, Sdringola S. Frequent diagnostic errors in cardiac PET/CT due to misregistration of CT attenuation and emission PET images: A definitive analysis of causes, consequences, and corrections. J Nucl Med 2007;48:1112–21.
20. Slomka PJ, Le Meunier L, Hayes SW, et al. Comparison of myocardial perfusion 82Rb PET performed with CT- and transmission CT-based attenuation correction. J Nucl Med 2008;49:1992–8.
21. Loghin C, Sdringola S, Gould KL. Common artifacts in PET myocardial perfusion images due to attenuation-emission misregistration: Clinical significance, causes, and solutions. J Nucl Med 2004;45:1029–39.
22. Alessio AM, Kohlmyer S, Branch K, Chen G, Caldwell J, Kinahan P. Cine CT for attenuation correction in cardiac PET/CT. J Nucl Med 2007;48:794–801.
23. Souvatzoglou M, Bengel F, Busch R, Kruschke C, Fernolendt H, Lee D, et al. Attenuation correction in cardiac PET/CT with three different CT protocols: A comparison with conventional PET. Eur J Nucl Med Mol Imaging 2007;34:1991–2000.
24. DiFilippo FP, Brunken RC. Do implanted pacemaker leads and ICD leads cause metal-related artifact in cardiac PET/CT? J Nucl Med 2005;46:436–43.
25. Hamill JJ, Brunken RC, Bybel B, DiFilippo FP, Faul DD. A knowledge-based method for reducing attenuation artefacts caused by cardiac appliances in myocardial PET/CT. Phys Med Biol 2006;51:2901–18.
26. Henzlova MJ, Duvall WL, Einstein AJ, Travin MI, Verberne HJ. ASNC imaging guidelines for SPECT nuclear cardiology procedures: Stress, protocols, and tracers. J Nucl Cardiol 2016;23:606–39.
27. Lieu HD, Shryock JC, von Mering GO, Gordi T, Blackburn B, Olmsted AW, et al. Regadenoson, a selective A2A adenosine receptor agonist, causes dose-dependent increases in coronary blood flow velocity in humans. J Nucl Cardiol 2007;14:514–20.
28. Johnson NP, Gould KL. Regadenoson versus dipyridamole hyperemia for cardiac positron emission tomography imaging. JACC Cardiovasc Imaging 2015;8:438–47.
29. Dilsizian V, Narula J. Capturing maximal coronary vasodilation for myocardial perfusion imaging: Timing is everything. JACC Cardiovasc Imaging 2015;8:499–500.
30. Sinusas AJ. Does a shortened hyperemia with regadenoson stress pose a concern for quantitative rubidium-82 PET imaging? Optimization of regadenoson PET imaging. JACC Cardiovasc Imaging 2015;8:448–50.
31. Dilsizian V, Gewirtz H, Paivanas N, et al. Serious and life threatening complications during cardiac stress testing: Potential mechanisms and management strategies. J Nucl Cardiol 2015;22:1198–213.
32. Bateman TM, Heller GV, McGhie AI, Friedman JD, Case JA, Bryngelson JR, et al. Diagnostic accuracy of rest/stress ECG-gated Rb-82 myocardial perfusion PET: Comparison with ECG-gated Tc-99m sestamibi SPECT. J Nucl Cardiol 2006;13:24–33.
33. Beanlands RS, Chow BJ, Dick A, Friedrich MG, Gulenchyn KY, Kiess M, et al. Canadian Cardiovascular Society, Canadian Association of Radiologists, Canadian Association of Nuclear Medicine, Canadian Nuclear Cardiology Society, Canadian Society of Cardiac Magnetic Resonance. CCS/CAR/CANM/CNCS/CanSCMR joint position statement on advanced noninvasive cardiac imaging using positron emission tomography, magnetic resonance imaging and multidetector computed tomographic angiography in the diagnosis and evaluation of ischemic heart disease-executive summary. Can J Cardiol 2007;23:107–19.
34. Dilsizian V, Taillefer R. Journey in evolution of nuclear cardiology: Will there be another quantum leap with the F-18 labeled myocardial perfusion tracers? JACC Cardiovasc Imaging 2012;5:1269–84.
35. Goldstein RA, Mullani NA, Marani SK, Fisher DJ, Gould KL, O'Brien HA Jr. Myocardial perfusion with rubidium-82. II. Effects of metabolic and pharmacologic interventions. J Nucl Med 1983;24:907–15.
36. Love WDB, Burch GE. Influence of the rate of coronary plasma on the extraction of rubidium-86 from coronary blood. Circ Res 1959;7:24–30.
37. Selwyn AP, Allan RM, L'Abbate A, Horlock P, Camici P, Clark J, et al. Relation between regional myocardial uptake of rubidium-82 and perfusion: Absolute reduction of cation uptake in ischemia. Am J Cardiol. 1982;50:112–21.
38. Senthamizhchelvan S, Bravo PE, Lodge MA, Merrill J, Bengel FM, Sgouros G. Radiation dosimetry of 82Rb in humans under pharmacologic stress. J Nucl Med 2011;52:485–91.
39. Hunter CR, Hill J, Ziadi MC, Beanlands RS, deKemp RA. Biodistribution and radiation dosimetry of (82)Rb at rest and during peak pharmacological stress in patients referred for myocardial perfusion imaging. Eur J Nucl Med Mol Imaging 2015;42:1032–42.
40. Hutchins GD, Schwaiger M, Rosenspire KC, Krivokapich J, Schelbert H, Kuhl DE. Noninvasive quantification of regional blood flow in the human heart using N-13 ammonia and dynamic positron emission tomographic imaging. J Am Coll Cardiol 1990;15:1032–42.
41. Krivokapich J, Smith GT, Huang SC, Hoffman EJ, Ratib O, Phelps ME, et al. 13N-ammonia myocardial imaging at rest and with exercise in normal volunteers. Quantification of absolute myocardial perfusion with dynamic positron emission tomography. Circulation 1989;80:1328–37.
42. Bergmann SR, Hack S, Tewson T, Welch MJ, Sobel BE. The dependence of accumulation of 13N-ammonia by myocardium on metabolic factors and its implications for quantitative assessment of perfusion. Circulation 1980;61:34–43.
43. Kitsiou AN, Bacharach SL, Bartlett ML, Srinivasan G, Summers RM, Quyyumi AA, et al. 13N-ammonia myocardial blood flow and uptake: Relation to functional outcome of asynergic regions after revascularization. J Am Coll Cardiol 1999;33:678–86.
44. Krivokapich J, Huang SC, Phelps ME, MacDonald NS, Shine KI. Dependence of myocardial extraction and clearance on flow and metabolism. Am J Physiol 1982;242:H536–42.

45. Hajjiri MM, Leavitt MB, Zheng H, Spooner AE, Fischman AJ, Gewirtz H. Comparison of positron emission tomography measurement of adenosine-stimulated absolute myocardial blood flow versus relative myocardial tracer content for physiological assessment of coronary artery stenosis severity and location. JACC Cardiovasc Imaging 2009;2:751–8.
46. Schindler TH, Schelbert HR, Quercioli A, Dilsizian V. Cardiac PET imaging for the detection and monitoring of coronary artery disease and microvascular health. JACC Cardiovasc Imaging 2010;3:623–40.
47. Schelbert HR, Phelps ME, Huang SC, MacDonald NS, Hansen H, Selin C, et al. N- 13 ammonia as an indicator of myocardial blood flow. Circulation 1981;63:1259–72.
48. International Commission on Radiological Protection. Radiation dose to patients from radiopharmaceuticals: ICRP publication 80. Ann IRCP 2000;28:113.
49. Bergmann SR, Fox KA, Rand AL, McElvany KD, Welch MJ, Markham J, et al. Quantification of regional myocardial blood flow in vivo with $H_2^{15}O$. Circulation 1984;70:724–33.
50. Bergmann SR, Herrero P, Markham J, Weinheimer CJ, Walsh MN. Noninvasive quantitation of myocardial blood flow in human subjects with oxygen-15-labeled water and positron emission tomography. J Am Coll Cardiol 1989;14:639–52.
51. Iida H, Kanno I, Takahashi A, Miura S, Murakami M, Takahashi K, et al. Measurement of absolute myocardial blood flow with $H_2^{15}O$ and dynamic positron-emission tomography. Strategy for quantification in relation to the partial-volume effect. Circulation 1988;78:104–15.
52. Danad I, Uusitalo V, Kero T, Saraste A, Raijmakers PG, Lammertsma AA, et al. Quantitative assessment of myocardial perfusion in the detection of significant coronary artery disease: Cutoff values and diagnostic accuracy of quantitative $[^{15}O]H_2O$ PET imaging. J Am Coll Cardiol 2014;64:1464–75.
53. Schindler TH, Dilsizian V. PET-determined hyperemic myocardial blood flow: Further progress to clinical application. J Am Coll Cardiol 2014;64:1476–8.
54. Nekolla SG, Reder S, Saraste A, Higuchi T, Dzewas G, Preissel A, et al. Evaluation of the novel myocardial perfusion positron-emission tomography tracer 18F-BMS-747158-02: Comparison to 13N-ammonia and validation with microsphere in a pig model. Circulation 2009;119:2333–42.
55. Dilsizian V. SPECT and PET myocardial perfusion imaging: Tracers and techniques. In: Dilsizian V, Narula J, editors. Atlas of nuclear cardiology. New York: Springer; 2013. p. 55–94.
56. Stanley WC, Lopaschuk GD, Hall JL, McCormack JG. Regulation of myocardial carbohydrate metabolism under normal and ischaemic conditions. Potential for pharmacological interventions. Cardiovasc Res 1997;33:243–57.
57. Gropler RJ, Siegel BA, Lee KJ, Moerlein SM, Perry DJ, Bergmann SR, et al. Nonuniformity in myocardial accumulation of fluorine-18-fluorodeoxyglucose in normal fasted humans. J Nucl Med 1990;31:1749–56.
58. Martin WH, Jones RC, Delbeke D, Sandler MP. A simplified intravenous glucose loading protocol for fluorine-18 fluorodeoxyglucose cardiac single-photon emission tomography. Eur J Nucl Med Mol Imaging 1997;24:1291–7.
59. Di Carli MF, Dorbala S, Meserve J, El Fakhri G, Sitek A, Moore SC. Clinical myocardial perfusion PET/CT. J Nucl Med 2007;48:783–93.
60. Strauss HW, Miller DD, Wittry MD, Cerqueira MD, Garcia EV, Iskandrian AS, et al. Procedure guideline for myocardial perfusion imaging 3.3. J Nucl Med Technol 2008;36:155–61.
61. Abraham A, Kass M, Ruddy TD, deKemp RA, Lee AK, Ling MC, et al. Right and left ventricular uptake with Rb-82 PET myocardial perfusion imaging: Markers of left main or 3 vessel disease. J Nucl Cardiol 2010;17:52–60.
62. Beanlands RS, Muzik O, Hutchins GD, Wolfe ER Jr, Schwaiger M. Heterogeneity of regional nitrogen 13-labeled ammonia tracer distribution in the normal human heart: Comparison with rubidium 82 and copper 62-labeled PTSM. J Nucl Cardiol 1994;1:225–35.
63. Cerqueira MD, Weissman NJ, Dilsizian V, Jacobs AK, Kaul S, Laskey WK, et al. American Heart Association Writing Group on Myocardial Segmentation and Registration for Cardiac Imaging. Standardized myocardial segmentation and nomenclature for tomographic imaging of the heart. A statement for healthcare professionals from the Cardiac Imaging Committee of the Council on Clinical Cardiology of the American Heart Association. J Nucl Cardiol 2002;9:240–5.
64. Gould KL, Johnson N, Bateman T, Beanlands RS, Bengel FM, Bober R, et al. Anatomic versus physiologic assessment of coronary artery disease: Guiding management decisions using positron-emission tomography (PET) as a physiologic tool. J Am Coll Cardiol 2013;62:1639–53.
65. Dilsizian V, Narula J. Qualitative and quantitative scrutiny by regulatory process: Is the truth subjective or objective? JACC Cardiovasc Imaging 2009;2:1037–8.
66. Flachskampf FA, Dilsizian V. Leaning heavily on PET myocardial perfusion for prognosis. JACC Cardiovasc Imaging 2014;7:288–91.
67. Nesterov SV, Deshayes E, Sciagra R, Settimo L, Declerck JM, Pan XB, et al. Quantification of myocardial blood flow in absolute terms using (82) Rb PET imaging: The RUBY-10 Study. JACC Cardiovasc Imaging 2014;7:1119–27.
68. Nakazato R, Berman DS, Dey D, Le Meunier L, Hayes SW, Fermin JS, et al. Automated quantitative Rb-82 3D PET/CT myocardial perfusion imaging: Normal limits and correlation with invasive coronary angiography. J Nucl Cardiol 2012;19:265–76.
69. Santana CA, Folks RD, Garcia EV, Verdes L, Sanyal R, Hainer J, et al. Quantitative (82)Rb PET/CT: Development and validation of myocardial perfusion database. J Nucl Med 2007;48:1122–8.
70. Chander A, Brenner M, Lautamaki R, Voicu C, Merrill J, Bengel FM. Comparison of measures of left ventricular function from electrocardiographically gated 82 Rb PET with contrast-enhanced CT ventriculography: A hybrid PET/CT analysis. J Nucl Med 2008;49:1643–50.
71. Parkash R, deKemp RA, Ruddy TD, Kitsikis A, Hart R, Beauchesne L, et al. Potential utility of rubidium 82 PET quantification in patients with 3-vessel coronary artery disease. J Nucl Cardiol 2004;11:440–9.
72. Ziadi MC, deKemp RA, Williams K, Guo A, Renaud JM, Chow BJ, et al. Does quantification of myocardial flow reserve using rubidium-82 positron emission tomography facilitate detection of multivessel coronary artery disease? J Nucl Cardiol 2012;19:670–80.
73. Herzog BA, Husmann L, Valenta I, Gaemperli O, Siegrist PT, Tay FM, et al. Long-term prognostic value of ^{13}N-ammonia myocardial perfusion positron emission tomography added value of coronary flow reserve. J Am Coll Cardiol 2009;54:150–6.
74. Murthy VL, Naya M, Foster CR, Hainer J, Gaber M, Di Carli G, et al. Improved cardiac risk assessment with noninvasive measures of coronary flow reserve. Circulation 2011;124:2215–24.
75. Ziadi MC, deKemp RA, Williams KA, Guo A, Chow BJ, Renaud JM, et al. Impaired myocardial flow reserve on rubidium-82 positron emission tomography imaging predicts adverse outcomes in patients assessed for myocardial ischemia. J Am Coll Cardiol 2011;58:740–8.
76. Lin JW, Laine AF, Akinboboye O, Bergmann SR. Use of wavelet transforms in analysis of time-activity data from cardiac PET. J Nucl Med 2001;42:194–200.

77. Lortie M, Beanlands RS, Yoshinaga K, Klein R, Dasilva JN, deKemp RA. Quantification of myocardial blood flow with 82Rb dynamic PET imaging. Eur J Nucl Med Mol Imaging 2007;34:1765–74.
78. El Fakhri G, Kardan A, Sitek A, Dorbala S, Abi-Hatem N, Lahoud Y, et al. Reproducibility and accuracy of quantitative myocardial blood flow assessment with (82)Rb PET: Comparison with (13)N-ammonia PET. J Nucl Med 2009;50:1062–71.
79. El Fakhri G, Sitek A, Guerin B, Kijewski MF, Di Carli MF, Moore SC. Quantitative dynamic cardiac 82Rb PET using generalized factor and compartment analyses. J Nucl Med 2005;46:1264–71.
80. Herrero P, Markham J, Shelton ME, Bergmann SR. Implementation and evaluation of a two-compartment model for quantification of myocardial perfusion with rubidium-82 and positron emission tomography. Circ Res 1992;70:496–507.
81. Herrero P, Markham J, Shelton ME, Weinheimer CJ, Bergmann SR. Noninvasive quantification of regional myocardial perfusion with rubidium-82 and positron emission tomography. Exploration of a mathematical model. Circulation 1990;82:1377–86.
82. Coxson PG, Huesman RH, Borland L. Consequences of using a simplified kinetic model for dynamic PET data. J Nucl Med 1997;38:660–7.
83. Yoshida K, Mullani N, Gould KL. Coronary flow and flow reserve by pet simplified for clinical applications using rubidium-82 or nitrogen-13-ammonia. J Nucl Med 1996;37:1701–12.
84. Dorbala S, Vangala D, Sampson U, Limaye A, Kwong R, Di Carli MF. Value of vasodilator left ventricular ejection fraction reserve in evaluating the magnitude of myocardium at risk and the extent of angiographic coronary artery disease: A 82Rb PET/CT study. J Nucl Med 2007;48:349–58.
85. Dorbala S, Hachamovitch R, Curillova Z, Thomas D, Vangala D, Kwong RY, et al. Incremental prognostic value of gated Rb-82 positron emission tomography myocardial perfusion imaging over clinical variables and rest LVEF. JACC Cardiovasc Imaging 2009;2:846–54.
86. Neely JR, Morgan HE. Relationship between carbohydrate and lipid metabolism and the energy balance of heart muscle. Ann Rev Physiol 1974;36:413–59.
87. Neely JR, Rovetto MJ, Oram JF. Myocardial utilization of carbohydrate and lipids. Prog Cardiovasc Dis 1972;15:289–329.
88. Stanley WC, Lopaschuk GD, McCormack JG. Regulation of energy substrate metabolism in the diabetic heart. Cardiovasc Res 1997;34:25–33.
89. Boudina S, Abel ED. Diabetic cardiomyopathy revisited. Circulation 2007;115:3213–23.
90. Taegtmeyer H, Dilsizian V. Imaging myocardial metabolism and ischemic memory. Nat Clin Pract Cardiovasc Med 2008;5(Suppl 2):S42–8.
91. Dilsizian V. FDG uptake as a surrogate marker for antecedent ischemia. J Nucl Med 2008;49:1909–11.
92. Kominsky DJ, Campbell EL, Colgan SP. Metabolic shifts in immunity and inflammation. J Immunol 2010;184:4062–8.
93. Hamacher K, Coenen HH, Stocklin G. Efficient stereospecific synthesis of no-carrier- added 2-[18f]-fluoro-2-deoxy-d-glucose using aminopolyether supported nucleophilic substitution. J Nucl Med 1986;27:235–8.
94. International Commission on Radiation Protection ICRP. Radiation dose to patients from radiopharmaceuticals – addendum 3 to ICRP publication 53. ICRP publication 106. Ann. ICRP 38 (1-2), 2008. International Commission on Radiation Protection website. http://www.icrp.org/publication.asp?id=ICRP%20Publication%20106. Accessed November 30, 2015.
95. Choi Y, Brunken RC, Hawkins RA, Huang SC, Buxton DB, Hoh CK, et al. Factors affecting myocardial 2-[F-18] fluoro-2-deoxy-d-glucose uptake in positron emission tomography studies of normal humans. Eur J Nucl Med Mol Imaging 1993;20:308–18.
96. Knuuti MJ, Nuutila P, Ruotsalainen U, Saraste M, Härkönen R, Ahonen A, et al. Euglycemic hyperinsulinemic clamp and oral glucose load in stimulating myocardial glucose utilization during positron emission tomography. J Nucl Med 1992;33:1255–62.
97. Dilsizian V, editor. Myocardial viability: A clinical and scientific treatise. New York: Futura Publishing Company, Inc.; 2000.
98. Heller GV, Links J, Bateman TM, Ziffer JA, Ficaro E, Cohen MC, et al. American Society of Nuclear Cardiology and Society of Nuclear Medicine Joint Position Statement: Attenuation correction of myocardial perfusion SPECT scintigraphy. J Nucl Cardiol 2004;11:229–30.
99. Malkerneker D, Brenner R, Martin WH, Sampson UK, Feurer ID, Kronenberg MW, et al. CT-based attenuation correction versus prone imaging to decrease equivocal interpretations of rest/stress Tc-99m tetrofosmin SPECT MPI. J Nucl Cardiol 2007;14:314–23.
100. Sandler MP, Videlefsky S, Delbeke D, Patton JA, Meyerowitz C, Martin WH, et al. Evaluation of myocardial ischemia using a rest metabolism/stress perfusion protocol with fluorine-18-fluorodeoxyglucose/technetium-99m-MIBI and dual-isotope simultaneous-acquisition single-photon emission computed tomography. J Am Coll Cardiol 1995;26:870–6.
101. Bax JJ, Visser FC, Blanksma PK, Veening MA, Tan ES, Willemsen TM, et al. Comparison of myocardial uptake of fluorine-18-fluorodeoxyglucose imaged with PET and SPECT in dyssynergic myocardium. J Nucl Med 1996;37:1631–6.
102. Dilsizian V, Bacharach SL, Muang KM, Smith MF. Fluorine-18-deoxyglucose SPECT and coincidence imaging for myocardial viability: Clinical and technological issues. J Nucl Cardiol 2001;8:75–88.
103. Srinivasan G, Kitsiou AN, Bacharach SL, Bartlett ML, Miller-Davis C, Dilsizian V. 18F-fluorodeoxyglucose single photon emission computed tomography: Can it replace PET and thallium SPECT for the assessment of myocardial viability? Circulation 1998;97:843–50.
104. Vitale GD, deKemp RA, Ruddy TD, Williams K, Beanlands RS. Myocardial glucose utilization and optimization of (18)F-FDG PET imaging in patients with non-insulin-dependent diabetes mellitus, coronary artery disease, and left ventricular dysfunction. J Nucl Med 2001;42:1730–6.
105. Ratib O, Phelps ME, Huang SC, Henze E, Selin CE, Schelbert HR. Positron tomography with deoxyglucose for estimating local myocardial glucose metabolism. J Nucl Med 1982;23:577–86.
106. Choi Y, Hawkins RA, Huang SC, Gambhir SS, Brunken RC, Phelps ME, Schelbert HR. Parametric images of myocardial metabolic rate of glucose generated from dynamic cardiac PET and 2-[18f]fluoro-2-deoxy-d-glucose studies. J Nucl Med 1991;32:733–8.
107. Beanlands RS, Hendry PJ, Masters RG, deKemp RA, Woodend K, Ruddy TD. Delay in revascularization is associated with increased mortality rate in patients with severe left ventricular dysfunction and viable myocardium on fluorine 18-fluorodeoxyglucose positron emission tomography imaging. Circulation 1998;98:II51–6.
108. Gerber BL, Ordoubadi FF, Wijns W, Vanoverschelde JL, Knuuti MJ, Janier M, et al. Positron emission tomography using (18)F-fluoro-deoxyglucose and euglycaemic hyperinsulinaemic glucose clamp: Optimal criteria for the prediction of recovery of post-ischaemic left ventricular dysfunction. Results from the European community concerted action multicenter study on use of

(18)F-fluoro-deoxyglucose positron emission tomography for the detection of myocardial viability. Eur Heart J 2001;22:1691–701.
109. Marshall RC, Tillisch JH, Phelps ME, Huang SC, Carson R, Henze E, et al. Identification and differentiation of resting myocardial ischemia and infarction in man with positron computed tomography, 18F-labeled fluorodeoxyglucose and N-13 ammonia. Circulation 1983;67:766–78.
110. Schwartz E, Schaper J, vom Dahl J, Altehoefer C, Buell U, Schoendube F, et al. Myocardial hibernation is not sufficient to prevent morphological disarrangements with ischemic cell alterations and increased fibrosis. Circulation 1994;30:I-378.
111. Tillisch J, Brunken R, Marshall R, Schwaiger M, Mandelkern M, Phelps M, et al. Reversibility of cardiac wall-motion abnormalities predicted by positron tomography. N Engl J Med 1986;314:884–8.
112. vom Dahl J, Altehoefer C, Sheehan FH, Buechin P, Uebis R, Messmer BJ, et al. Recovery of regional left ventricular dysfunction after coronary revascularization. Impact of myocardial viability assessed by nuclear imaging and vessel patency at follow-up angiography. J Am Coll Cardiol 1996;28:948–58.
113. Thompson K, Saab G, Birnie D, Chow BJ, Ukkonen H, Ananthasubramaniam K, et al. Is septal glucose metabolism altered in patients with left bundle branch block and ischemic cardiomyopathy? J Nucl Med 2006;47:1763–8.
114. Ben-Haim S, Gacinovic S, Israel O. Cardiovascular infection and inflammation. Semin Nucl Med 2009;39:103–14.
115. James OG, Christensen JD, Wong TZ, Borges-Neto S, Koweek LM. Utility of FDG PET/CT in inflammatory cardiovascular disease. Radiographics 2011;31:1271–86.
116. Kandolin R, Lehtonen J, Kupari M. Cardiac sarcoidosis and giant cell myocarditis as causes of atrioventricular block in young and middle-aged adults. Circ Arrhythm Electrophysiol 2011;4:303–9.
117. Takano H, Nakagawa K, Ishio N, Daimon M, Daimon M, Kobayashi Y, et al. Active myocarditis in a patient with chronic active Epstein-Barr virus infection. Int J Cardiol 2008;130:e11–3.
118. Greulich S, Deluigi CC, Gloekler S, Wahl A, Zürn C, Kramer U, et al. CMR imaging predicts death and other adverse events in suspected cardiac sarcoidosis. JACC Cardiovasc Imaging 2013;6:501–11.
119. Koiwa H, Tsujino I, Ohira H, Yoshinaga K, Otsuka N, Nishimura M. Images in cardiovascular medicine: Imaging of cardiac sarcoid lesions using fasting cardiac ^{18}F- fluorodeoxyglucose positron emission tomography: An autopsy case. Circulation 2010;122:535–6.
120. Silverman KJ, Hutchins GM, Bulkley BH. Cardiac sarcoid: A clinicopathologic study of 84 unselected patients with systemic sarcoidosis. Circulation 1978;58:1204–11.
121. Matsui Y, Iwai K, Tachibana T, Fruie T, Shigematsu N, Izumi T, et al. Clinicopathological study of fatal myocardial sarcoidosis. Ann N Y Acad Sci 1976;278:455–69.
122. Hiraga H, Hiroe M, Iwai K, et al. Guideline for diagnosis of cardiac sarcoidosis: Study report on diffuse pulmonary diseases. Tokyo: The Japanese Ministry of Health and Welfare; 1993. p. 23–4 in Japanese.
123. Diagnostic standard and guidelines for sarcoidosis. Jpn J Sarcoidosis Granulomatous Disord 2007;27:89–102.
124. Tahara N, Tahara A, Nitta Y, Kodama N, Mizoguchi M, Kaida H, et al. Heterogeneous myocardial FDG uptake and the disease activity in cardiac sarcoidosis. JACC Cardiovasc Imaging 2010;3:1219–28.
125. Mc Ardle BA, Leung E, Ohira H, Cocker MS, deKemp RA, DaSilva J, et al. The role of (18F)-fluorodeoxyglucose positron emission tomography in guiding diagnosis and management in patients with known or suspected cardiac sarcoidosis. J Nucl Cardiol 2013;20:297–306.
126. Schatka I, Bengel FM. Advanced imaging of cardiac sarcoidosis. J Nucl Med 2014;55:99–106.
127. Skali H, Schulman AR, Dorbala S. ^{18}F-FDG PET/CT for the assessment of myocardial sarcoidosis. Curr Cardiol Rep 2013;15:352.
128. Youssef G, Leung E, Mylonas I, Nery P, Williams K, Wisenberg G, et al. The use of ^{18}F-FDG PET in the diagnosis of cardiac sarcoidosis: A systematic review and metaanalysis including the Ontario experience. J Nucl Med 2012;53:241–8.
129. Birnie D. HRS expert consensus statement on the diagnosis and management of arrhythmias associated with cardiac sarcoidosis. Heart Rhythm 2014;11:1305–23.
130. Ohira H, Tsujino I, Ishimaru S, Oyama N, Takei T, Tsukamoto E, et al. Myocardial imaging with ^{18}F-fluoro-2-deoxyglucose positron emission tomography and magnetic resonance imaging in sarcoidosis. Eur J Nucl Med Mol Imaging 2008;35:933–41.
131. Blankstein R, Osborne M, Naya M, Waller A, Kim CK, Murthy V, et al. Cardiac positron emission tomography enhances prognostic assessments of patients with suspected cardiac sarcoidosis. J Am Coll Cardiol 2014;63:329–36.
132. Langah R, Spicer K, Gebregziabher M, Gordon L. Effectiveness of prolonged fasting ^{18}F-FDG PET-CT in the detection of cardiac sarcoidosis. J Nucl Cardiol 2009;16:801–10.
133. Harisankar CN, Mittal BR, Agrawal KL, Abrar ML, Bhattacharya A. Utility of high fat and low carbohydrate diet in suppressing myocardial FDG uptake. J Nucl Cardiol 2011;18:926–36.
134. Williams G, Kolodny GM. Suppression of myocardial ^{18}F-FDG uptake by preparing patients with a high-fat, low-carbohydrate diet. AJR Am J Roentgenol 2008;190:W151–6.
135. Lum DP, Wandell S, Ko J, Coel MN. Reduction of myocardial 2-deoxy-2-[18F] fluoro-d- glucose uptake artifacts in positron emission tomography using dietary carbohydrate restriction. Mol Imaging Biol 2002;4:232–7.
136. Persson E. Lipoprotein lipase, hepatic lipase and plasma lipolytic activity. Effects of heparin and a low molecular weight heparin fragment (Fragmin). Acta Med Scand 1988;724:1–56.
137. Manabe O, Yoshinaga K, Ohira H, Masuda A, Sato T, Tsujino I, et al. The effects of 18-h fasting with low-carbohydrate diet preparation on suppressed physiological myocardial 18F-fluorodeoxyglucose (FDG) uptake and possible minimal effects of unfractionated heparin use in patients with suspected cardiac involvement sarcoidosis. J Nucl Cardiol 2015;23:244–52.
138. Asmal AC, Leary WP, Thandroyen F, Botha J, Wattrus S. A dose-response study of the anticoagulant and lipolytic activities of heparin in normal subjects. Br J Clin Pharmacol 1979;7:531–3.
139. Schleipman AR, Gerbaudo VH. Occupational radiation dosimetry assessment using an automated infusion device for positron-emitting radiotracers. J Nucl Med Technol 2012;40:244–8.
140. Blankstein R, Budoff MJ, Shaw LJ, Goff DC Jr, Polak JF, Lima J, et al. Predictors of coronary heart disease events among asymptomatic persons with low low-density lipoprotein cholesterol mesa (multi-ethnic study of atherosclerosis). J Am Coll Cardiol 2011;58:364–74.
141. Okumura W, Iwasaki T, Toyama T, Iso T, Arai M, Oriuchi N, et al. Usefulness of fasting ^{18}F-FDG PET in identification of cardiac sarcoidosis. J Nucl Med 2004;45:1989–98.
142. Ishimaru S, Tsujino I, Takei T, Tsukamoto E, Sakaue S, Kamigaki M, et al. Focal uptake on FDG PET tomography images indicates cardiac involvement of sarcoidosis. Eur Heart J 2005;26:1538–43.
143. Bartlett ML, Bacharach SL, Voipio-Pulkki LM, Dilsizian V. Artifactual inhomogeneities in myocardial PET and SPECT scans in normal subjects. J Nucl Med 1995;36:188–95.

144. Dweck MR, Jones C, Joshi NV, Fletcher AM, Richardson H, White A, et al. Assessment of valvular calcification and inflammation by positron emission tomography in patients with aortic stenosis. Circulation 2012;125:76–86.
145. Ahmadian A, Brogan A, Berman J, Sverdlov AL, Mercier G, Mazzini M, et al. Quantitative interpretation of FDG PET/CT with myocardial perfusion imaging increases diagnostic information in the evaluation of cardiac sarcoidosis. J Nucl Med 2014;21:925–39.
146. Osborne MT, Hulten EA, Singh A, Waller AH, Bittencourt MS, Stewart GC, et al. Reduction in ^{18}F-fluorodeoxyglucose uptake on serial cardiac positron emission tomography is associated with improved left ventricular ejection fraction in patients with cardiac sarcoidosis. J Nucl Cardiol 2014;21:166–74.
147. Uslan DZ, Sohail MR, St Sauver JL, Friedman PA, Hayes DL, Stoner SM, et al. Permanent pacemaker and implantable cardioverter defibrillator infection: A population-based study. Arch Intern Med 2007;167:669–75.
148. Sandoe JA, Barlow G, Chambers JB, Gammage M, Guleri A, Howard P, et al. Guidelines for the diagnosis, prevention and management of implantable cardiac electronic device infection. Report of a joint working party project on behalf of the British Society for Antimicrobial Chemotherapy (BSAC, host organization), British Heart Rhythm Society (BHRS), British Cardiovascular Society (BCS), British Heart Valve Society (BHVS) and British Society for Echocardiography (BSE). J Antimicrob Chemother 2015;70:325–59.
149. Chu VH, Crosslin DR, Friedman JY, Reed SD, Cabell CH, Griffiths RI, et al. Staphylococcus aureus bacteremia in patients with prosthetic devices: Costs and outcomes. Am J Med 2005;118:1416.
150. Chen W, Kim J, Molchanova-Cook OP, Dilsizian V. The potential of FDG PET/CT for early diagnosis of cardiac device and prosthetic valve infection before morphologic damages ensue. Curr Cardiol Rep 2014;16:459.
151. Bensimhon L, Lavergne T, Hugonnet F, Mainardi JL, Latremouille C, Maunoury C, et al. Whole body [(18) F] fluorodeoxyglucose positron emission tomography imaging for the diagnosis of pacemaker or implantable cardioverter defibrillator infection: A preliminary prospective study. Clin Microbiol Infect 2011;17:836–44.
152. Sarrazin JF, Philippon F, Tessier M, Guimond J, Molin F, Champagne J, et al. Usefulness of fluorine-18 positron emission tomography/computed tomography for identification of cardiovascular implantable electronic device infections. J Am Coll Cardiol 2012;59:1616–25.
153. Saby L, Laas O, Habib G, Cammilleri S, Mancini J, Tessonnier L, et al. Positron emission tomography/computed tomography for diagnosis of prosthetic valve endocarditis: Increased valvular ^{18}F-fluorodeoxyglucose uptake as a novel major criterion. J Am Coll Cardiol 2013;61:2374–82.
154. Schouten LR, Verberne HJ, Bouma BJ, van Eck-Smit BL, Mulder BJ. Surgical glue for repair of the aortic root as a possible explanation for increased F-18 FDG uptake. J Nucl Cardiol 2008;15:146–7.
155. Dilsizian V, Achenbach S, Narula J. On adding versus selecting imaging modalities for incremental diagnosis: A case-study of ^{18}F-fluorodeoxyglucose PET/CT in prosthetic valve endocarditis. JACC Cardiovasc Imaging 2013;6:1020–1.
156. Pagano D, Townend JN, Littler WA, Horton R, Camici PG, Bonser RS. Coronary artery bypass surgery as treatment for ischemic heart failure: The predictive value of viability assessment with quantitative positron emission tomography for symptomatic and functional outcome. J Thorac Cardiovasc Surg 1998;115:791–9.
157. Beanlands RS, Nichol G, Huszti E, Humen D, Racine N, Freeman M, et al. F-18-fluorodeoxyglucose positron emission tomography imaging- assisted management of patients with severe left ventricular dysfunction and suspected coronary disease: A randomized, controlled trial (PARR-2). J Am Coll Cardiol 2007;50:2002–12.
158. Di Carli MF, Davidson M, Little R, Khanna S, Mody FV, Brunken RC, et al. Value of metabolic imaging with positron emission tomography for evaluating prognosis in patients with coronary artery disease and left ventricular dysfunction. Am J Cardiol 1994;73:527–33.